The Pennsylvania State University

The J. Jeffrey and Ann Marie Fox Graduate School

HEAT-MODIFIED BIOCHAR FOR Pb IMMOBILIZATION IN SOIL

A Thesis in

Soil Science

by

Cara Melissa Bintrim

Submitted in Partial Fulfillment
of the Requirements
for the Degree of

Master of Science

December 2025

The thesis of Cara Melissa Bintrim was reviewed and approved by the following:

Ekaterina Bazilevskaya
Assistant Research Professor of Soil Chemistry
Thesis Advisor

John Spargo
Research Professor
Director of Agricultural Analytical Services Laboratory

Mary Ann Bruns
Professor Emerita of Soil Microbiology

Isabel Fendley
Assistant Research Professor of Geosciences

Patrick Drohan
Professor of Pedology
Director of Graduate Studies of Soil Science

ABSTRACT

Soil lead (Pb) contamination is often a barrier to safe urban agriculture in the Northeastern U.S., with health risks tied to the bioaccessible Pb fraction. This study evaluates whether low-temperature heat-treatment can significantly modify biochar for greater Pb sorption and therefore reduction of Pb bioaccessibility in contaminated soils. First, we characterized and evaluated the Pb sorption capacity of wood-chip biochar heated in air at 300°C. Then, using the EPA Method 1340 in-vitro bioaccessibility assay, we performed three experiments: (1) a trial 13-week study with heated and unheated biochars and one soil, (2) an expanded 2-month study with four biochar types and two soils, and (3) an investigation of moisture effects on unheated biochar performance in one soil kept at three soil water contents. Our results suggest that while heat treatment did significantly alter the physical and chemical properties of biochar and enhance its Pb sorption capacity, the modified biochar was not consistently effective in reducing Pb exposure risk within the soil environment.

In addition to biochar modification, this study assesses benchtop energy-dispersive X-ray fluorescence (EDXRF, hereafter XRF) spectroscopy as a lower-cost alternative for measuring Pb in liquid environmental samples. Liquid-phase extractions are widely used to assess Pb solubility and bioaccessibility in soils, but these solutions are typically analyzed using Inductively Coupled Plasma Optical Emission Spectroscopy (ICP-OES, hereafter ICP), a sensitive yet costly technique requiring specialized facilities and expertise. Accurate quantification of lead (Pb) in environmental samples is essential for evaluating contamination risks and guiding remediation, especially in urban soils affected by legacy pollution.

This study assesses XRF spectroscopy for measuring Pb in three solution types:

1. EPA Method 1340 extracts (in vitro gastric-soluble Pb)
2. $Pb(NO_3)_2$ solutions (used in biochar-Pb sorption studies)
3. Mehlich 3 extracts (for nutrient and trace metal screening).

Regression analyses comparing XRF and ICP showed strong agreement (r^2 = 0.9835 - 0.9985) across all matrices. XRF detection limits (the smallest amount of analyte detectable by the instrument) ranged from 0.17 to 0.25 mg L^{-1}, with quantification limits (the smallest amount of analyte reliably quantified by the instrument) between 0.51 and 0.75 mg L^{-1}. Average measurement reproducibility was high (standard deviation 0.055–1.50, depending on solution type). These findings indicate that XRF offers a reliable, rapid, and cost-effective approach for quantifying Pb in aqueous extracts, thus extending its applicability to community laboratories, field-based research, and contexts with limited analytical infrastructure. While XRF has traditionally been employed for solid matrices, its demonstrated performance with liquid extracts underscores its potential to broaden the scope of environmental testing beyond conventional applications.

TABLE OF CONTENTS

LIST OF FIGURES

LIST OF TABLES

ACKNOWLEDGEMENTS

This material is based upon work supported by the Pennsylvania Department of Agriculture (grant #C940001083); the National Institute of Food and Agriculture, U.S. Department of Agriculture, through the Northeast Sustainable Agriculture Research and Education program under subaward number GNE24-327; and the College of Agricultural Sciences at the Pennsylvania State University. Any opinions, findings, conclusions, or recommendations expressed in this publication are those of the author and do not necessarily reflect the view of the Pennsylvania Department of Agriculture, the U.S. Department of Agriculture, the Pennsylvania State University, or the College of Agricultural Sciences. Additionally, any mention of trade names or commercial products within this research is solely intended to provide specific information and should not be interpreted as a recommendation or endorsement by the College of Agricultural Sciences or the Pennsylvania State University.

I would also like to thank my advisor, Katya Bazilevskaya, for her help and my thesis committee—Mary Ann Bruns, Isabel Fendley, John Spargo, and Patrick Drohan—for their guidance throughout my time at Penn State. Additionally, I'd like to thank Sage Schmouder for being a helping hand and friend during long hours in lab; Ondi Brown, Anna Perederina, and Michael Robbins for their help keeping SRCL up and running; and my classmates and friends Stephen Dadio, Helen Senerchia, and Duke Williams for their kindness as I began a degree in a field that was completely new to me. In my coursework, Dr. Jennifer Weld, Dr. Sridhar Komarneni, and Prof. Brian Morris instilled a love of soil science and teaching. This work would not be possible without the help of the staff at the Penn State Agricultural Analytical Services Laboratory, Carlos Leon y Leon at Phospholutions, Pat Sherren at Metzler Biochar, and Darren Parmer at the Green & Healthy Homes Initiative. Finally, I would like to thank my parents, Beth and Tim; my sisters Sylvia and Wendy; and my grandparents Tom and Sue for their support throughout my studies.

Chapter 1

Introduction

Description of project focus

Urban agriculture and gardening are important for community well-being, offering clear social and economic advantages to low-income communities (Hanna & Oh, 2000; Horst et al., 2017). Urban agriculture fosters neighborhood engagement, stimulates local economies, and enhances access to fresh produce. However, a major challenge facing urban agriculture is soil contamination with heavy metals, particularly lead (Pb), which remains a legacy contaminant (Lusby et al., 2015; O'Shea et al., 2021). When assessing urban sites for agriculture, stakeholders must develop reliable risk assessment approaches and choose robust and sustainable mitigation strategies (Kim et al., 2014; Wagner & Payne, 2019; Wharton et al., 2012).

Conventional approaches to mitigating Pb pollution in soil include removal, physical encapsulation, dilution, chemical treatment, electrokinetic remediation, and, more recently, phytoremediation techniques (Priya et al., 2023). In comparison, the use of biochar as an agent for soil remediation has received less attention (Amalina et al., 2022; Bashir et al., 2020a), likely due to the fact that biochars exhibit a tremendous variety in properties. It is important to note that not all biochars are equal, and some may have better capability to retain Pb than others (Sivaranjanee et al., 2023; Tan & Yu, 2023). The reactivity of biochar can be enhanced through activation procedures, which include physical, chemical, and thermal methods (Amalina et al., 2022; Bashir et al., 2020). Increases in biochar reactivity can improve their ability to remove heavy metals from solution. In urban agriculture communities, compost additions are a commonly used approach to reduce ("dilute") Pb concentration in soil, but there are limitations. Compost additions may not be effective for soils with high concentrations of Pb.

Moreover, previous research has indicated that compost may not efficiently retain Pb in the soil; instead, compost could increase Pb's mobility, potentially leading to Pb discharge into groundwater during decomposition processes (Bolan et al., 2014). In fact, relying solely on compost as a remediation approach can lead to nutrient overapplication and potential runoff of excessive nutrients to nearby streams (Small et al., 2019).

As opposed to compost, biochar demonstrates promise as a remediation material, exhibiting high efficiency in Pb retention due to its abundant surface area and reactive functional groups (Yuan et al., 2019). Activation methods can be used to functionalize (i.e. add functional groups to) biochars to improve their reactivity. However, some of the procedures employed to manufacture commercial activated biochars may involve strong chemicals and should be conducted at a large commercial facility (Yuan et al., 2019). An alternative method, air oxidation, has shown promise for increasing biochar porosity and surface oxygenation of biochar without the use of chemical reagents (Sun et al., 2022).

In this study, we evaluate an inexpensive method to functionalize biochar and increase its reactivity towards Pb: heating biochar at 300°C under an air environment. We hypothesize that heating biochar in the presence of oxygen for several hours will activate its surface, creating more surface functional groups and making it more reactive towards Pb adsorption. We will test this hypothesis in a laboratory setting by characterizing physical and chemical changes to the biochar, performing aqueous Pb sorption experiments, and finally testing bioaccessible Pb in soil amended with the biochar. If the heated biochar does show superior Pb-sorbing properties, it follows that such a product would provide significant economic and health benefits as a soil amendment for urban gardeners.

To evaluate the efficacy of biochar amendment, we will assess whether functionalized biochar reduces bioaccessible Pb levels. While the EPA regulates total Pb concentration, this measure may not accurately reflect the potential health risks related only to the Pb readily available for absorption by the human body. An *in vitro* bioaccessibility method, such as EPA Method 1340 (US EPA, 2017), will allow us to estimate the portion of Pb that can be absorbed by humans and therefore provide a better

understanding of its risk. Moreover, to enhance the accessibility and affordability of this analysis, we seek to develop a procedure for analyzing EPA Method 1340 assays using X-ray fluorescence (XRF) spectroscopy. Unlike the costly and labor-intensive Inductively Coupled Plasma (ICP) analysis, XRF offers a more accessible and rapid alternative, aligning with our goal to make bioaccessibility assays more rapid, feasible and affordable, especially for laboratories serving underprivileged urban communities.

To summarize, if functionalized biochar proves to considerably decrease Pb bioaccessibility in soil (preferably, to below 60% bioaccessibility (US EPA, 2007)), its use could be beneficial for urban gardeners to mitigate the risk of Pb poisoning for themselves, their children, and their entire communities. In alignment with this objective, we are also validating a novel, rapid and cost-effective analytical method for quantifying the amount of Pb in liquid soil extracts.

Heavy metal contamination in urban soils

Pb is a heavy metal occurring naturally in the soil environment at levels below 50 ppm (Pourrut et al., 2011), comprising 0.002% of Earth's crust (Kumar et al., 2022). Anthropogenic Pb contamination in soils is typically found in the soil surface, as Pb is not easily translocated within the profile (Pais & Jones, 1998; Pourrut et al., 2011). While Pb is of industrial utility, it does not have a biological use in living cells and in fact has toxic effects on organisms (Pourrut et al., 2011).

Pb is infamous for its negative impacts on human health. In the human body, Pb causes cardiovascular and renal disease in adults, as well as pregnancy complications and loss. In children, Pb is particularly dangerous to the nervous system, causing irreversible neurological damage (Laidlaw & Filippelli, 2008). Children also have increased vulnerability due to higher absorption of Pb via the gastrointestinal tract (Yan et al., 2016).

There are many possible routes of Pb exposure. Inhalation of Pb fumes and dusts is a common occupational hazard in industrial settings such as smelting and recycling plants (Levin, 2016).

Contaminated products such as foods, packaging, children's toys, and jewelry may also introduce Pb into the body. Pb-containing plumbing can cause Pb poisoning via drinking water, whereas Pb-containing paint can produce flakes and dusts that may be inhaled or ingested. One of the primary environmental sources of exposure, and of interest in this study, is soil containing elevated levels of Pb (Mielke et al., 2022; *Sources of Lead Exposure*, 2023).

In urban environments, Pb contamination in soil typically originates from four main sources: roads, buildings with Pb paint, industrial sites, and toxic waste sites (Schupp et al., 2020). Soils along roadways have accumulated Pb through past leaded gasoline emissions, while Pb paints were once commonly used in residential areas and may enter the soil by chipping off of existing painted surfaces or demolition and renovation residues (Huang et al., 2024). Pb can be present in the soil at levels exceeding 10,000 ppm in areas affected by Pb paint scrapings (Zia et al., 2011). Industrial sites and persistent wastes near residential or recreational areas may also contribute to exposure (H. Huang et al., 2024).

In addition to their increased susceptibility to and damage from Pb poisoning, children are behaviorally more likely than adults to consume Pb. Children may consume Pb-contaminated soil by putting their hands into their mouths after playing in soil or participating in gardening activities. Alternatively, children may eat the soil directly or consume produce grown in contaminated garden soil (Byers et al., 2020). Exposure to Pb by eating thoroughly washed vegetables and fruits is not considered to be the most likely route, as uptake is low in most plant species and Pb is less likely to be absorbed on a full stomach (Laidlaw et al., 2016).

Agricultural community

According to the U.S. Centers for Disease Control, children from low-income families and certain racial and ethnic groups have a higher risk of exposure to Pb (*Childhood Lead Poisoning Prevention: Populations at Higher Risk*, 2021). Pb is present in higher concentrations in soils of poor communities,

often situated in older buildings and located near former industrial sites (Whitehead & Buchanan, 2019). At the same time, urban gardening is being promoted as a biophilic solution to food insecurity and as a means of social development in cities (*Urban Agriculture*, n.d.).

The U.S. Environmental Protection Agency defines environmental justice as follows:

> "Environmental justice" means the just treatment and meaningful involvement of all people, regardless of income, race, color, national origin, Tribal affiliation, or disability, in agency decision-making and other Federal activities that affect human health and the environment so that people:
>
> - are fully protected from disproportionate and adverse human health and environmental effects (including risks) and hazards, including those related to climate change, the cumulative impacts of environmental and other burdens, and the legacy of racism or other structural or systemic barriers; and
> - have equitable access to a healthy, sustainable, and resilient environment in which to live, play, work, learn, grow, worship, and engage in cultural and subsistence practices (US EPA, 2024b).

Pb exposure is an environmental hazard disproportionately affecting urban children, who are thus limited in their access to healthy spaces to experience the outdoors and garden alongside their elders. Many residents in urban neighborhoods rely on gardens for their food supply or recreational areas, particularly for children. Assessing Pb levels in soils and demonstrating the effectiveness of amendments such as biochar for bioaccessible Pb mitigation could help residents to protect their families from potential Pb exposure through activities like playing or gardening in contaminated soil.

This project aims primarily to benefit urban gardeners and their families who grow produce in areas with historical industrial activity or urban pollution, such as those in the City of Lancaster, PA. By understanding the levels of bioaccessible Pb and total Pb in their soils, growers can make informed decisions about potential risks and appropriate soil management practices.

Testing soils for total Pb

Determining the amount of Pb in soil can be done using a method such as X-ray fluorescence (XRF) or EPA Method 3050B and inductively coupled plasma optical emission spectroscopy (ICP-OES) (*Lead in Soil*, 2020; *Soil Contaminants: Lead*, 2024). The U.S. EPA has recommended 400 ppm as the maximum Pb level for children's play areas and 1,200 ppm standard elsewhere on the property (*Lead in Soil*, 2020), but a 2024 news release announced the maximum for residential properties has been reduced to 200 ppm (US EPA, 2024a). However, due to the nature of the soil and the chemical form of the Pb therein, only a portion of the total Pb may be dangerous to human health.

In soil, Pb can exist as a monoatomic cation, within inorganic or organic complexes, or adsorbed onto soil colloids and organic matter (Pourrut et al., 2011). The fraction of ingested Pb that is potentially physiologically soluble to an organism is termed "bioaccessible" (US EPA, 2021). Various soil properties can influence the form of Pb present, its solubility, and therefore its bioaccessibility (Pourrut et al., 2011). Soil pH is significant in that bioaccessible Pb is higher in soils with lower pH than in more alkaline soils, as H^+ ions tend to compete with Pb cations for binding sites and less soluble Pb carbonates are formed at higher pH (Yang et al., 2003; Zia et al., 2011). Soil organic matter, mineralogy, cation exchange capacity (CEC), and redox conditions all affect the bioaccessibility of Pb. For example, organic ligands or iron oxides may bind to Pb species and reduce their availability (Pourrut et al., 2011; Zia et al., 2011). Phosphorus content of soil is also known to improve immobilize Pb by forming insoluble pyromorphite (Zia et al., 2011).

Testing soils for bioaccessible Pb

Compared to measures of total Pb, *in vitro* bioaccessibility (IVBA) assays allow for more precise estimation of the risks to human health by exposure to a particular soil. This information is useful because a soil containing high Pb levels does not necessarily correlate to elevated Pb concentrations in the blood

of people living in that area, as the Pb may be immobilized in the soil. Because of the effects of Pb poisoning on children's nervous systems, and because the primary exposure pathway for children is ingestion, these assays typically aim to mimic the conditions of the digestive system (Huang et al., 2023; Zia et al., 2011). While there is no federal regulatory limit for bioaccessible Pb, the U.S. EPA suggests that if the measured relative bioaccessibility of a soil is above 60%, the soil may be more dangerous than might be assumed based on total Pb (US EPA, 2007).

Five *in vitro* laboratory procedures for measuring bioaccessibility of Pb in soil have been published, some measuring bioaccessibility in fluids mimicking the environment of the stomach, intestines, or duodenum, as well as in saliva or bile (Yan et al., 2016). A procedure called the Relative Bioavailability Leaching Procedure (RBALP), uses a solution buffered with 0.4 M glycine at 37°C and a pH of 1.5 to estimate gastric bioaccessibility (Drexler & Brattin, 2007). The human stomach varies between a pH of 1 and 4 when fasting, and the average human body temperature is 37°C. The U.S. EPA *in vitro* Pb bioaccessibility procedure, EPA Method 1340, outlines a standardized version of RBALP (US EPA, 2017).

Benchtop XRF for measuring bioaccessible Pb

Compared to measures of total Pb, *in vitro* bioaccessibility assays give more precise estimation of risks to human health by exposure to a particular soil. Because one of the most dangerous effects of Pb poisoning is damage to children's nervous systems, and because the primary exposure pathway for children is ingestion, these assays typically aim to mimic the conditions of the digestive system (Zia et al., 2011). The U.S. EPA Method 1340 uses a solution buffered with 0.4 M glycine at 37°C and a pH of 1.5 to estimate gastric bioaccessibility. Traditionally, the concentration of Pb extracted into the solution is measured via ICP (EPA Method 6010 or 6020) (US EPA, 2017). However, Paltseva and Cheng (2018) proposed combining simplified bioaccessibility assays with analysis by portable X-ray fluorescence

(pXRF). Similar to benchtop XRF, pXRF is non-destructive and far less complex and costly compared to ICP. In the hopes of making simple bioaccessibility assays functional in the field and available to less well-equipped labs, Paltseva and Cheng tested several extractions with both ICP and pXRF. pXRF results on standard solutions were systematically 15% higher than expected (Paltseva & Cheng, 2018).

Paltseva and Cheng's research suggests the possibility of simplifying and reducing costs of Pb testing for liquid environmental samples. Although their research found some limitations of portable XRF, it is worth investigating whether functional results can be achieved with benchtop XRF for a non-destructive, simple, and less costly technique as compared to traditional ICP methods.

In addition to EPA Method 1340, Mehlich 3, a standard soil nutrient and trace metal extraction, has gained popularity as a proxy for estimating bioaccessible Pb (Minca et al., 2013). Mehlich 3 extractants are also typically measured by ICP-OES, so we chose to include this solution type as well for XRF testing. Additionally, simple aqueous $Pb(NO_3)_2$ solutions, commonly used in soil spiking for laboratory experiments, were chosen for XRF method development.

Biochar for remediation of heavy metals

There are multiple ways in which biochar is able to immobilize heavy metals in the soil, through both direct and indirect interactions. Direct interactions include electrostatic attraction (in which electronegative biochar surface groups attract cations), ion exchange (in which biochars exchange surface cations for heavy metal cations), complexation (in which heavy metals form complexes with biochar functional groups) and precipitation (in which components of the biochar form insoluble precipitates with heavy metals). Biochar can have indirect effects by changing the soil composition and increasing the soil pH, cation exchange capacity (CEC), and organic carbon content, all of which affect metal mobility in the soil (He et al., 2019). Biochar can add elements such as phosphorus and carbon to the soil, which readily form insoluble precipitates with Pb (Yang et al., 2021). Due to its alkalinity, biochar can significantly

increase soil pH with repeated applications. This change in pH causes soil particles to have a greater net negative charge, which attracts heavy metal cations and thus makes them less bioaccessible in the soil solution (Rees et al., 2014).

Methods of modifying biochar following production can involve chemical treatments to increase functional groups on the biochar surface. For example, Behnam et al. investigated using H_2SO_4/HNO_3 treatment to functionalize biochar for Pb sorption in aqueous systems (Behnam et al., 2024), while Bashir et al. used KOH-treated biochar for sorption of cadmium in soil (Bashir et al., 2020a). Both studies found favorable results using functionalized biochar for metal uptake. In our research, we aim to functionalize biochar using heat in the presence of oxygen, with the goal of achieving similar results without the use of harsh chemical treatment.

Chapter 2

Thermal Oxidation of Biochar for Enhancing Pb Sorption

Introduction

Biochar can immobilize heavy metals in the soil through both direct and indirect interactions. Direct interactions include electrostatic attraction (in which electronegative biochar surface groups attract cations), ion exchange (in which biochars exchange surface cations for heavy metal cations), complexation (in which heavy metals form complexes with biochar functional groups), and precipitation (in which components of the biochar form insoluble precipitates with heavy metals). Biochar can have indirect effects by changing the soil composition and increasing the soil pH, cation exchange capacity (CEC), and organic carbon content, all of which affect metal mobility in the soil (He et al., 2019). Biochar can also add elements such as phosphorus and carbon to the soil, which readily form insoluble precipitates with lead (X. Yang et al., 2021b). Biochar can significantly increase soil pH with repeated applications. This change in pH causes soil particles to have a greater net negative charge, which attracts heavy metal cations and thus makes them less bioaccessible in the soil solution (Rees et al., 2014).

While biochar's capacity to immobilize heavy metals is well established, post-production oxidative functionalization can increase surface acidity and binding site density, potentially enhancing metal uptake. Methods of modifying biochar following production can involve chemical treatments to increase functional groups on the biochar surface. For example, Behnam et al. (2024) investigated using H_2SO_4/HNO_3 treatment to functionalize biochar for lead sorption in aqueous systems, while Bashir et al. (2020) used KOH-treated biochar for sorption of cadmium in soil. Both studies found favorable results using functionalized biochar for metal uptake. However, chemical treatments generally involve the use of hazardous reactants that increase treatment costs and raise environmental concerns related to their safe

disposal. In our research, we hope to functionalize biochar using heat in the presence of oxygen, with the goal of achieving similar results without the use of harsh chemical treatments.

To test our hypothesis that heat-functionalized biochar will sorb Pb more effectively due to changes in its structure and surface functional groups, we heated wood chip biochar for increasing lengths of time in air at 300°C. We then analyzed the heated and unheated samples for changes in chemical and structural properties (pH, surface area, porosity, and functional groups). Finally, we conducted Pb adsorption experiments at moderate pH (5-6) to investigate whether functionalized biochar was able to attract Pb in solution at better rates than unheated biochar.

Methods

Biochar source

Wood residues from the forestry industry are one of the most common materials used for biochar feedstocks (Zhao et al., 2019). Wood chip biochar ("PureChar Fine") was sourced from Metzler Biochar in Reedsville, PA, with the company providing product characterization (included in the Appendix). Metzler biochar is produced from mixed hardwood (a common feedstock) with pyrolysis conditions of 704.4˚C for 30 min in the absence of oxygen. The biochar was used as-received.

Biochar treatment

Approximately 4 cups of the biochar was heated on 30 cm x 30.5 cm x 4 cm cast iron trays in a Thermolyne tabletop muffle furnace (model type: F30400) in air at 300°C for varying lengths of time (1 hour, 2 hours, 3 hours, and 4 hours, excluding preheating time) at a 40°C/min heating rate. The trays were

covered with perforated aluminum foil to prevent displacement of the biochar but allow air flow. After cooling in the furnace, the samples were transferred to paper cartons and stored in a desiccator.

Characterization

We characterized the heated biochars and an unheated sample based on pH, surface area/pores, and functional groups. Biochar pHs were measured using a glass electrode pH probe following (Rajkovich et al., 2012) (recommended by the International Biochar Initiative): a 1:20 biochar:water w/v slurry. Biochar surface area and pore size distribution were analyzed by the Brunauer-Emmet-Teller (BET) and Density Functional Theory (DFT) methods (Thommes et al., 2015), using a Micromeritics 3Flex gas sorption analyzer. Biochar samples were outgassed at 150˚C and analyzed by nitrogen sorption at 77 K. Functional groups were determined by Fourier Transform Infrared Spectroscopy (FTIR) using a Thermo Scientific spectrometer with an attenuated total reflectance (ATR) accessory and OMNIC software for spectrum analysis. Functional groups selection and assignments were based on data from Leon y Leon & Radovic, 1993. We measured four functional group types: phenolic groups (C-O bond at wavenumber 1079 cm^{-1}), aromatic groups (C-H bond at wavenumber 874 cm^{-1}), carboxyl groups (C=O bond at wavenumber 1584 cm^{-1}) and carbonyl groups (C=O bond at wavenumber 1422 cm^{-1}).

Based on the characterization results, we decided to omit the 2-hour heated biochar from further experiments, as it did not show large differences from the 3-hour heated biochar. The 3-hour heated biochar was chosen for further experiments as it showed that large differences from the unheated biochar could be achieved at a moderate heating time, therefore reducing energy and time requirements for production.

Sorption experiment

Sorption experiments were conducted using unheated and 3-hour heated biochars. Approximately 0.1 g of biochar (with 3 experimental replicates) was added to 50 mL of solution, corresponding to a solid:solution ratio equal to 2 g L^{-1} Solutions consisted of ASTM Type I water with varying concentrations of $Pb(NO_3)_2$: 0, 50, 100, 150, 200, 300, 400, 500, 600, and 700 mg L^{-1} made using Sigma Aldrich lead (II) nitrate (ACS reagent grade, ≥ 99.0%).

The pH of each mixture was checked after 1.5 hours of shaking and remained between 5 and 6. The samples were then shaken overnight (18 h) at room temperature before filtration through 1) a Whatman 2 filter paper to remove large solids and 2) a 0.45 µm syringe filter to remove particulates. The filtered solutions were then stored at 4°C until their analysis by energy dispersive X-ray fluorescence (EDXRF) using a Rigaku NEX CG II Series analyzer with liquid sample cup holders (see Chapter 4 for method description).

Sorption isotherms were analyzed using the Langmuir model (Thommes et al., 2015):

$$V = \frac{V_m K_{eq} C_{eq}}{1 + K_{eq} C_{eq}}$$

where C_{eq} is the equilibrium Pb concentration in solution (mg L^{-1}), V is the Pb adsorbed to the biochar at equilibrium (mg g^{-1}), V_m is the monolayer adsorption saturation capacity (mg g^{-1}), and K_{eq} (L mg^{-1}) is the Langmuir model constant. Triplicate data were averaged for the final isotherm graphs.

Statistical analysis

A paired t-test was conducted comparing the amount of Pb sorbed from each $Pb(NO_3)_2$ solution by unheated biochar and 3-hour heated biochar. All assumptions were met, and differences were normally distributed (Anderson-Darling p-value = 0.260). The null hypothesis was that the mean difference between Pb absorbed by heated and unheated biochar was equal to zero. Minitab software was used with a 95% confidence level (Minitab, LLC, 2023).

Results

Biochar average pH decreased significantly with heating time: from pH 10.51 ± 0.01 for unheated biochar, pH 9.34 ± 0.03 for 1 hour of heating, pH 9.02 ± 0.03 for 2 hours of heating, pH 9.06 ± 0.03 for 3 hours of heating, and pH 8.72 ± 0.03 for 4 hours of heating (Figure 2-1).

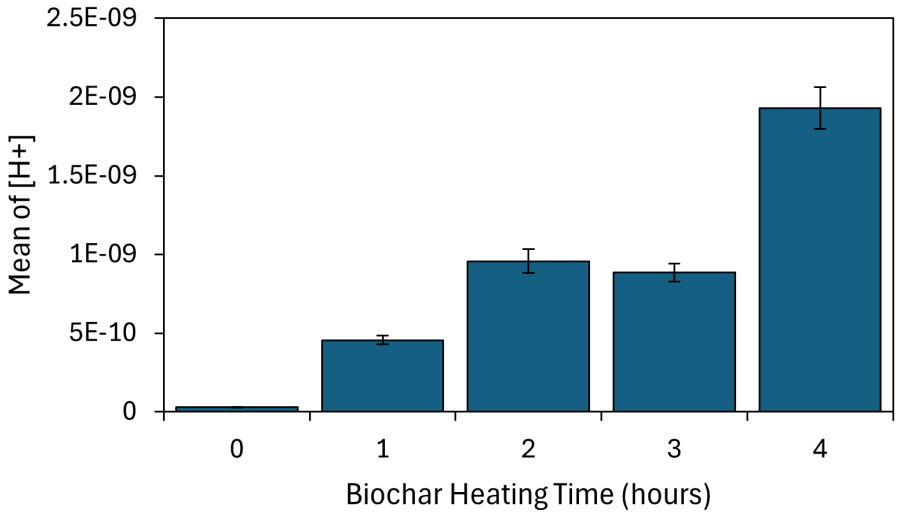

Figure 2-1: Bar chart of hydrogen ion concentrations calculated from pH data for unheated and heated biochars. Error bars represent standard error from three replicates.

The total surface area of the biochar also changed with heating time, increasing from 503.18 m^2g^{-1} in unheated biochar to 633.4 m^2g^{-1} in 4-hour heated biochar (Table 2-1).

Table 2-1. Surface area and pore analysis results (using Brunauer–Emmett–Teller (BET) and Density Functional Theory (DFT) methods) for the unheated and heated biochar samples.

Heating time (h)	Surface area (m^2g^{-1})				Pore volume (cm^3g^{-1})			Avg pore size (Gurvich) (nm)
	Total (BET)	Micropores (t-Plot)	External (t-Plot)	Percent Micropores	Total	Micropores	Percent Micropores	
0	503.18	493.03	10.14	97.98	0.230	0.212	92.14	1.83
1	604.48	593.20	11.27	98.14	0.284	0.264	93.11	1.88
2	612.79	599.86	12.93	97.89	0.293	0.270	92.15	1.91
3	623.72	612.16	11.56	98.15	0.297	0.277	93.23	1.90
4	633.40	619.54	13.86	97.81	0.306	0.281	91.93	1.93

Figure 2-2 shows a gas adsorption isotherm plotting nitrogen adsorbed vs. relative pressure for unheated biochar and biochars heated for 1, 2, and 3 hours. The height of the curve on the y axis indicates more gas adsorbed, while the shape of the curve on the x axis is associated with the sizes of slit-shape pores typical of carbon materials. The first plateau shows the range of micropores, the second plateau shows mesopores, and finally macropores towards 0.95 P/Po (Thommes et al., 2015). At any given P/Po, a higher curve means more gas adsorbed (greater accessible surface/pore volume); here the samples rank 3h = 2h > 1h ≫ 0h.

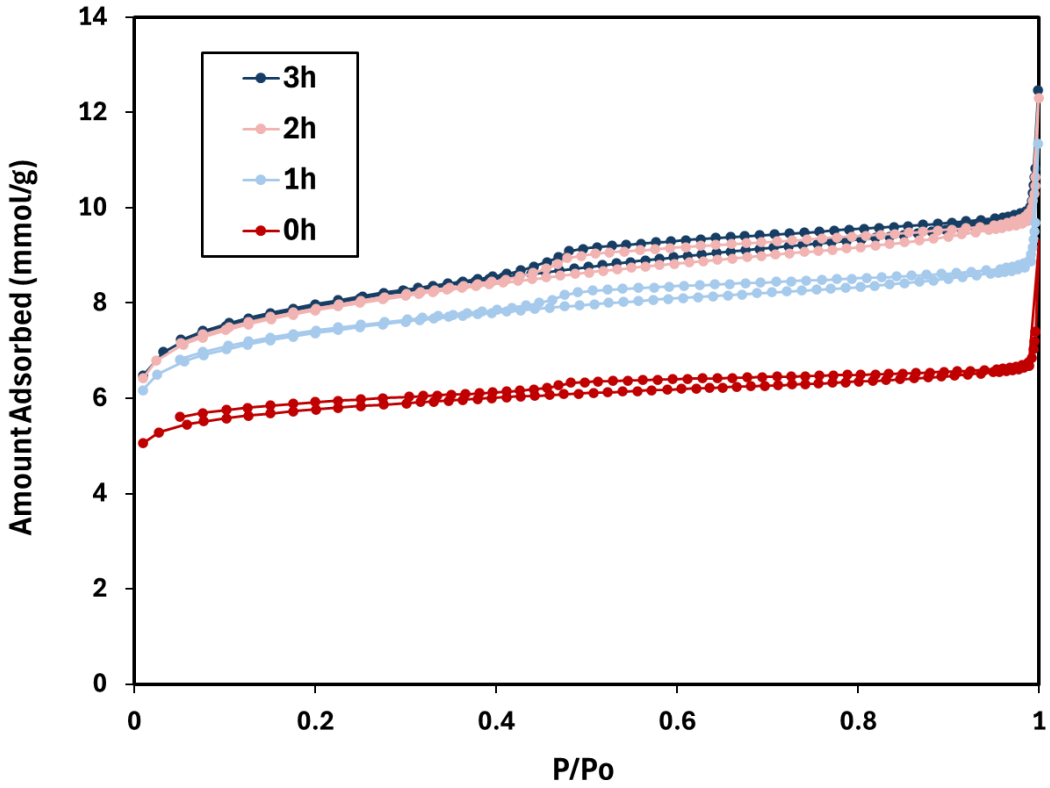

Figure 2-2. Brunauer–Emmett–Teller (BET) physisorption isotherm used in determining the surface areas of different biochars. Source: Carlos Leon y Leon.

Figure 2-3 plots pore volume vs. pore size for unheated biochar and biochars heated for 1, 2, and 3 hours. While pore size remained consistent, pore volume was increased steadily by heating.

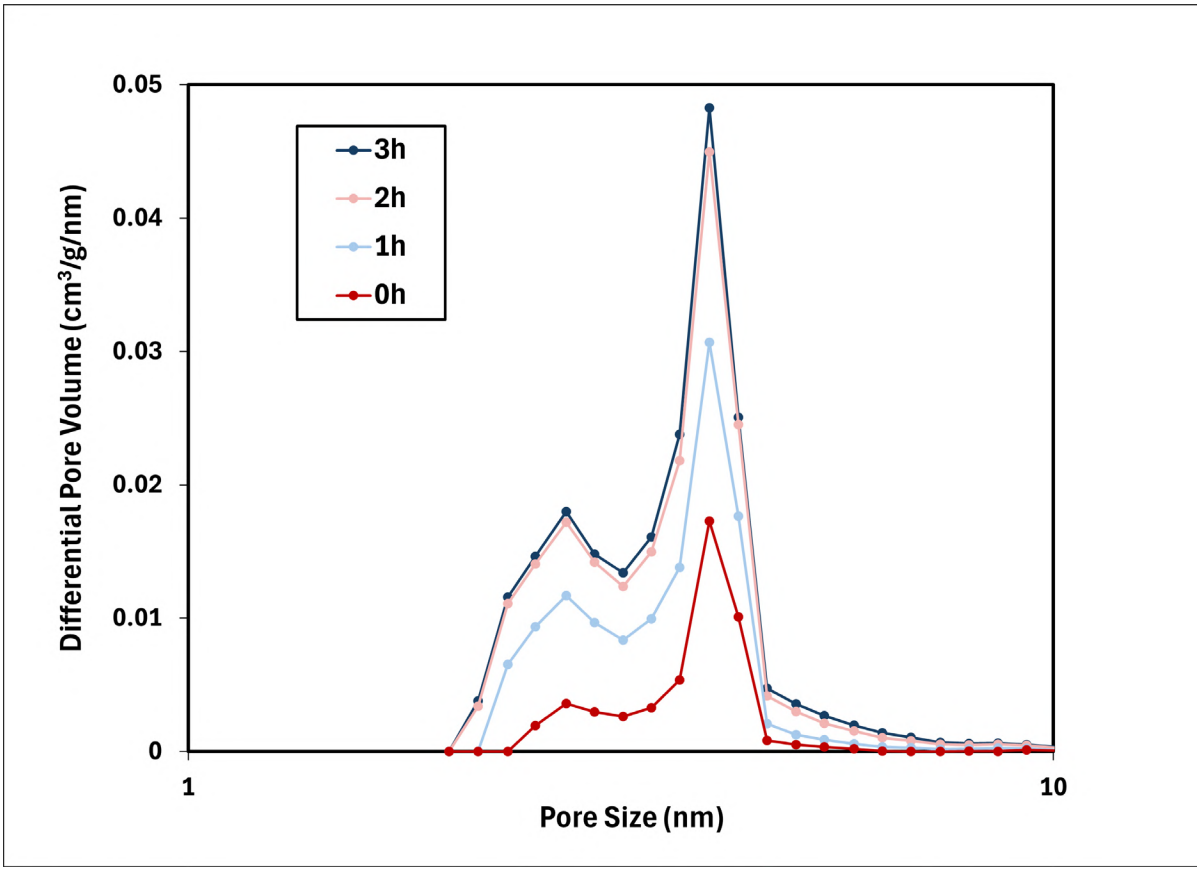

Figure 2-3. Chart showing differential pore volume vs. pore size for different biochars. Differential pore volume ($cm^3\ g^{-1}\ nm^{-1}$) is pore volume per unit pore diameter; peak height shows the most abundant pore sizes. Source: Carlos Leon y Leon.

IR spectroscopy showed that, with the exception of the 2-hour heated biochar, heating tended to decrease the proportion of phenolic and aromatic groups (wavenumbers 1079 cm^{-1} and 874 cm^{-1}) and increase the more acidic carboxyl and carbonyl groups (wavenumbers 1584 cm^{-1} and 1422 cm^{-1}) (Figure 2-4).

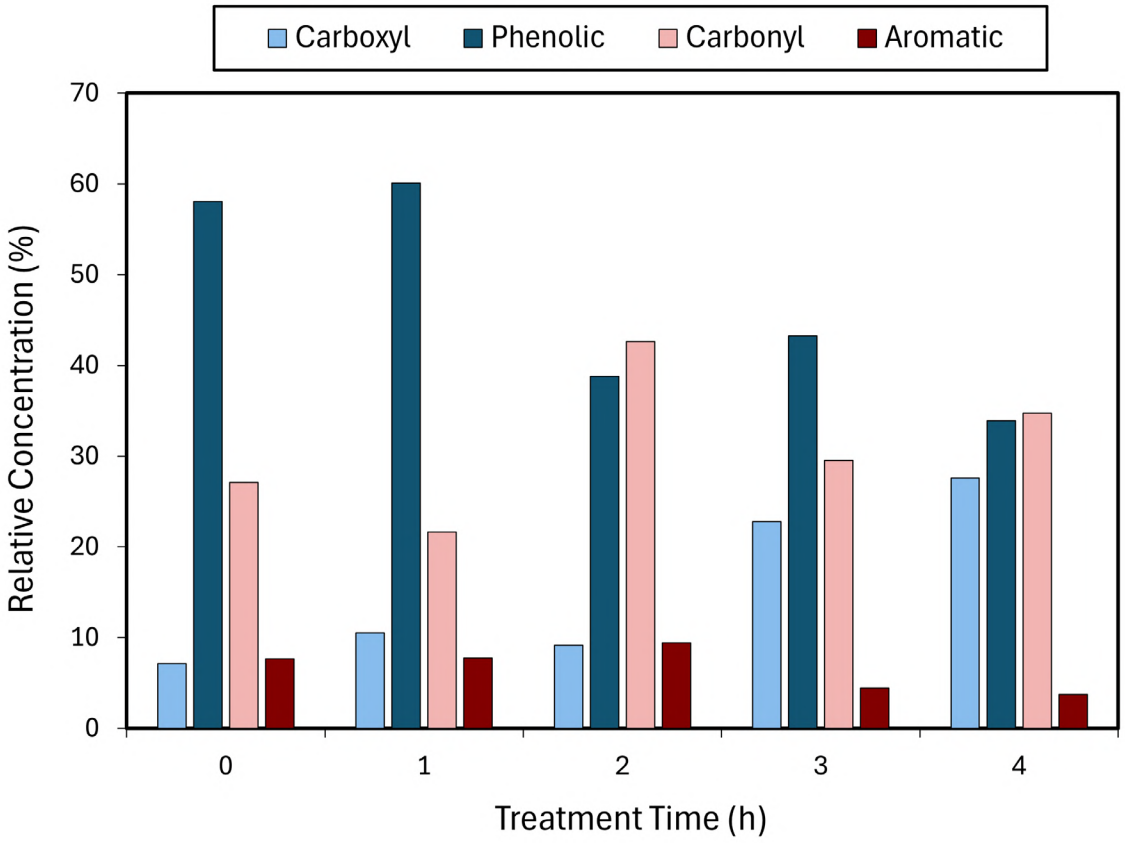

Figure 2-4. Bar chart displaying the relative proportions of acidic functional groups in decreasing order of acidity (carboxyl, carbonyl, phenolic, and aromatics) measured on unheated and heated biochar samples by FTIR. Source: Carlos Leon y Leon.

In the sorption experiment, a paired t-test comparing the amount of Pb adsorbed to the biochars gave a p-value of >0.001 for a mean difference of 16.46 (19.90, 13.03). At the 5% significance level, we rejected the null hypothesis that the mean difference was equal to 0 and, from the positive confidence interval, concluded that heated biochar had a higher sorption of Pb than unheated biochar in each $Pb(NO_3)_2$ solution.

A sorption isotherm using the Langmuir model showed a K_{eq} (the Langmuir equilibrium constant, an estimate of the affinity of the sorbate to the sorbent) of 0.34 L mg^{-1} and a V_m (monolayer adsorption saturation capacity) of 55.07 g kg^{-1} Pb for unheated biochar (Figure 2-5). The isotherm for 3-hour heated biochar had a K_{eq} of 4.58 L mg^{-1} and V_m of 72.96 g kg^{-1} Pb (Figure 2-5). Adsorption values were more

variable in the last 2-3 samples. Variability and higher Pb adsorption values could potentially be due to underestimation of Pb concentrations if Pb fell out of solution in the more concentrated samples.

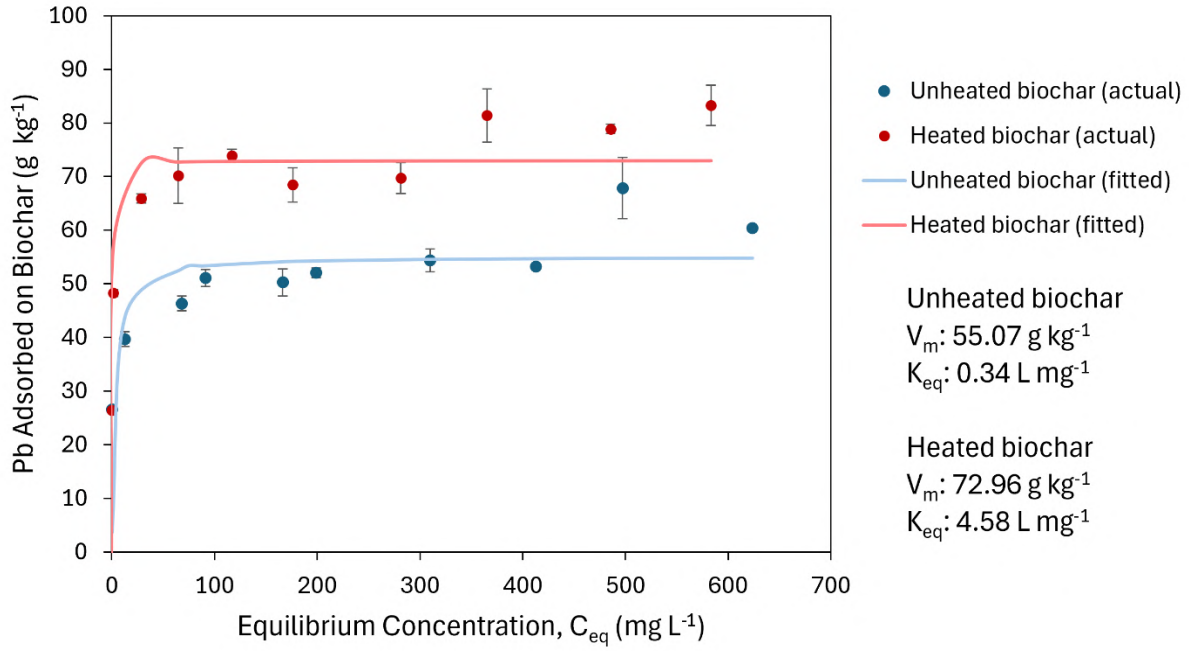

Figure 2-5. Langmuir isotherms showing Pb (as aqueous $Pb(NO_3)_2$) adsorption onto unheated and 3-hour heated wood chip biochar. For unheated biochar $R^2 = 0.9974$, and for heated biochar $R^2 = 0.9968$.

Discussion

Heated biochars showed lower pH (Figure 2-1), greater surface area (Table 2-1 and Figure 2-2), a higher volume of similarly sized pores (Figure 2-3), and a different proportion of certain functional groups (Figure 2-4) as compared to the control unheated biochar. These results show that heating biochar in air at a relatively low temperature (300˚C) can cause chemical and physical changes to the material, which could potentially create a higher affinity for Pb ions. Specifically, the shifting of the predominant acidic functional group (phenolic) to a stronger acid (carboxylic) could explain the pH change and allow better sorption of Pb cations. This result is similar to the findings of Xie et al. (2017), who demonstrated that chemically introducing oxygen functional groups (carboxyl and hydroxyl) helped increase copper

adsorption on walnut shell biochar by 77.68%. However, it is noteworthy that Xie et al. introduced oxygen functionalities through sequential treatments with harsh chemicals (H_3PO_4 at 500˚C followed by HNO_3 at 80˚C), which are much more hazardous and costly than the simpler air oxidation treatments contemplated in our study (Xie et al., 2017).

Between heat treatments, in 3- and 4-hour heated biochars, the pH decreased steadily as the heating time was increased (Figure 2-1). However, the 2-hour heated biochar had a slightly lower average pH than the 3-hour heated sample (pH 9.021 ± 0.034 compared to pH 9.055 ± 0.029, with an instrument precision of ± 0.001 units). While this small difference could be due to sample heterogeneity, this pattern was also seen in the FTIR data: 2-hour heated biochar had a lower proportion of carboxyl groups and higher aromatic and carbonyl functional groups than was expected based on the trends seen in the other treatments (Figure 2-4). As oxygen reacts with the biochar surface, pore openings might initially shrink due to oxygen blocking pore entrances, but perhaps after 3 hours of heating, the pores are widened enough by the removal of other functional groups to allow oxygen to attack the inner pore walls. Otherwise, the 2-hour heated biochar did behave as expected, with porosity, pore volume, and surface area intermediate between that of 1- and 3-hour heated samples (Figures 2-2 and 2-3).

The sorption experiment focusing on 3-hour heated biochar supported the hypothesis that heating can help increase the attraction of Pb ions to biochar. The paired t-test comparing heated and unheated biochar Pb sorption in each $Pb(NO_3)_2$ solution showed greater adsorption to heated biochar ($p > 0.001$).

With a larger K_{eq}, the heated biochar had a stronger attraction between adsorbate and adsorbent, and the larger V_m shows that more Pb was adsorbed onto the heated biochar. As shown in Figure 2-5, the Langmuir isotherm for Pb sorption onto unheated biochar reaches maximum adsorption at around 55.07 mg Pb (g biochar)$^{-1}$, while that of the heated biochar reaches maximum adsorption at 72.96 mg Pb (g biochar)$^{-1}$.

The practical implications of these findings need further exploration to determine if the functionalization effects improve biochar's Pb removal significantly in the field. Future concerns may

also include batch consistency when heating biochar in air; perhaps a replicate of our 2-hour heated sample may have given more consistent results. Additionally, heterogeneity of the sample, different heating methods (a different heating vessel shape or placement in the furnace may affect the evenness of heating), and different types of biochar (produced from different feedstocks and/or under different conditions) may be explored. More research is needed to determine whether increased porosity or functional group bonding is the predominant mechanism of Pb immobilization. Further, we need to measure the strength of the treated biochar's Pb retention, which could be accomplished through desorption experiments. Remaining limitations include the need to replicate the observed 2-h treatment discrepancies; corroborate our pH and FTIR surface-chemistry inferences with measurements of pH_{pzc} (pH at the point of zero charge), Boehm titrations, and/or XPS; and evaluate robustness under more realistic conditions that include competing cations/anions and desorption or bioaccessibility tests. Determining how this biochar behaves in Pb-contaminated wastewater or soil can elucidate its utility in the field of environmental remediation. Chapter 3: "Functionalized biochar for reducing in-vitro bioaccessible Pb in soil" explores the addition of heated biochar to the more complicated system of soil samples. In soil, the presence of other sorbents (e.g. clays or organic matter), competitive cations, a diversity of Pb forms, fluctuating moisture levels, microbial activity, and other factors may play a role in the reaction of Pb ions with biochar.

Conclusions

Oxidizing a wood chip-based biochar in air at 300˚C produced a measurable transformation of surface chemistry and texture, lowering suspension pH, increasing specific surface area and pore development, and shifting FTIR signatures toward more oxygenated functionalities. These modifications were accompanied by systematically greater Pb sorption capacity and apparent affinity in batch tests, with conventional isotherm models sufficiently capturing the data.

Taken together, the evidence supports a mechanistic interpretation in which added acidic sites (e.g., –COOH/–C=O) strengthen specific interactions with Pb(II) beyond what can be attributed to solution pH alone. To explicitly separate pH effects from functionalization effects, future work will employ pH-edge experiments at fixed ionic strength and initial concentration, reporting pH_{50} as a compact metric of low-pH affinity.

Dissolved Pb in filtrates was measured by EDXRF for throughput and consistency with the larger project; detailed calibration, quality assurance, and XRF↔ICP regression validation are provided in Chapter 4. Collectively, these results indicate that low-temperature oxidative functionalization is a practical strategy to enhance the Pb-binding performance of biochar for environmental applications. Industrial-scale implementation of this biochar modification appears feasible; however, future work will evaluate whether the added costs are justified by the net gains in Pb immobilization efficiency.

Chapter 3

Functionalized Biochar for Reducing Bioaccessible Pb

Introduction

A major hurdle to popularizing urban agriculture in the Northeastern US is potential soil contamination by heavy metals, especially legacy contaminants like lead (Pb). Measurements of total Pb can be misleading since actual health risks depend on the human intake rate and the fraction of Pb that is bioavailable. We estimate this fraction by measuring in-vitro bioaccessible Pb—the amount of Pb released into solution when soil is subjected to conditions similar to the human digestive tract (US EPA, 2017). Amendments for remediating contaminated soil, such as biochar, are well-known for their metal-sorbing properties, but should be tested for their effectiveness in specifically reducing Pb bioaccessibility (Sivaranjanee et al., 2023; Tan & Yu, 2023). Even if an amendment is proven to sorb Pb, it should be determined whether Pb resists desorption from the material and is made non-accessible to humans.

Biochar attracts metal ions through physical and chemical interactions. Many methods, primarily involving chemical treatments, can activate biochar to increase these interactions (Amalina et al., 2022; Bashir et al., 2020b). We propose using heat instead of chemical reagents to treat biochar. Biochar characterization results (Chapter 2) indicate that post-processing air-heating of biochar increases the abundance of oxygen-containing surface functional groups and, consequently, its capacity to sorb Pb from solution. However, soils are heterogeneous systems: native organic matter, clay minerals, and iron (hydr)oxides provide competing sorption sites, and environmental conditions (e.g., pH, redox status, moisture, dissolved organic carbon) can either promote Pb sorption or, conversely, increase Pb solubility (Dong et al., 2000; Li, Liu, et al., 2023; Sauvé et al., 1998). To test the performance of the heat-treated biochar, we measured the fraction of bioaccessible Pb in amended and unamended soils using the U.S.

EPA Method 1340 in-vitro bioaccessibility assay (US EPA, 2017). We hypothesize that due to its increased porosity and surface functional groups, heat-treated biochar will significantly reduce Pb bioaccessibility in amended soil compared to unamended soil or soil amended with untreated biochar.

We address this hypothesis in three steps. **Experiment 1** tested whether low-temperature air-heating (300 °C) of a wood-chip biochar changes soil Pb in-vitro bioaccessibility (IVBA) relative to unheated biochar, using a 5% w/w amendment in a Pb-contaminated urban soil and sampling over 13 weeks. **Experiment 2** scaled and generalized the approach across two soils with contrasting total Pb (~260 and ~720 mg kg^{-1}), applied 2% w/w biochar heated for 1, 3, or 4 hours, and tracked IVBA dynamics from 1 day to 2 months to evaluate variability across matrices and treatments. **Experiment 3** then isolated a key environmental control—moisture—by comparing IVBA below, at, and above field capacity (~10%, ~23%, ~47% gravimetric) with and without 2% biochar, investigating whether moisture/redox conditions mediate the efficacy of the amendment.

Experiment 1: Heated biochar trial experiment

Objective

To test whether heat-treated biochar can reduce Pb bioaccessibility in soil, we performed a small trial experiment using unamended contaminated soil, soil amended with unheated biochar, and soil amended with biochar heated at 300°C for three hours. Pb in-vitro bioaccessibility (IVBA) was determined using EPA Method 1340 over several timepoints spanning 13 weeks.

Methods

Wood chip biochar was sourced from Metzler Biochar in Reedsville, PA, with the company providing product characterization (Appendix). Functionalized biochar was prepared by heating 80-mL ceramic crucibles of biochar in air to 300°C for three hours in a muffle furnace. The pH of both heated and unheated biochar was measured as well as surface area and pore volume. For biochar pH, we followed the procedure recommended by the International Biochar Initiative: 1:20 biochar:water w/w (Rajkovich et al., 2012). Surface area and pore volume were determined by Brunauer–Emmett–Teller (BET) and Density Functional Theory (DFT) methods.

Soil was collected from a community garden site in Philadelphia, PA, in 2022 (Dadio, S., 2024). The soil was dried and sieved to 2 mm. It was a sandy loam texture (hydrometer method with sand sieving from Gee & Bauder, 1986; Gee & Or, 2018) with a pH of 7.44 (1:1 w/w water:soil) and 6.5% organic matter (loss on ignition method, Schulte & Hoskins, 2011). The total lead concentration was measured as 510.78 mg kg^{-1} following EPA Methods 3050B and 6010B (US EPA, 1996a, 1996b).

32 g of soil was placed into each of 36 plastic 50-mL beakers. The beakers were divided into three treatments: control soil, soil with 5% w/w unheated biochar, and soil with 5% w/w heated biochar. Biochar was mixed into the dry soil until evenly distributed. The total lead in the unheated and heated biochar mixtures was estimated to be 486.46 mg kg^{-1}, assuming negligible Pb in the 5% biochar. Each beaker was covered in perforated parafilm and maintained at 40% moisture by mass with weekly checks.

At approximately 0, 2, 8, and 13 weeks, one beaker of each of the three treatments was removed for bioaccessibility and pH tests. The EPA Method 1340: In-Vitro Bioaccessibility (IVBA) Assay for Lead in Soil procedure was used (following the 2013 revision, soil was sieved to 250 μm) (US EPA, 2017). The resulting extracts were tested by EPA Method 6010B on ICP-OES (MDL = 0.005 and LOQ = 0.025) (US EPA, 1996b). IVBA calculations were carried out as follows: (Extracted Pb*100)/(Total Pb * Mass of Sample). Note that due to experimental error and the nature of the IVBA calculation (the total Pb value is also derived from a soil extraction), some IVBA percentages can exceed 100%. Nonparametric

statistical analyses (Kruskal-Wallis and Dunn's tests) were used due to small sample sizes, and statistical significance was determined at the 5% level. Graphs were constructed in R (version 4.4.1) using the ggplot2 package (Kassambara, 2025).

Results

Biochar pH decreased from 10.26 to 8.79 following 3 hours of heating. The surface area also increased from 502.76 m^2/g to 659.24 m^2/g (31.1% change), while pore volume increased from 0.227 cm^3/g to 0.336 cm^3/g (48.0% change).

The Kruskal-Wallis test was used with the null hypothesis that the median Pb IVBA values at each sampling timepoint were equal. In each treatment, the Kruskal-Wallis p-value was less than 0.05, so the null hypothesis was rejected (Table 3-1) and a Dunn's post hoc test was used to determine which timepoints differed. In all three treatments, Pb IVBA was significantly lower at Time 1 (1 day) than at Time 2 (2 weeks) (see Table 3-2 and Figure 3-1 panels A-C). After 8 weeks (Times 3-4), Pb IVBA seemed to stabilize and did not change significantly.

Table 3-1. Kruskal-Wallis test results for comparing differences in Pb in-vitro bioaccessibility (IVBA) between sampling times (degrees of freedom = 3).

Treatment	N	Time 1 Median IVBA (%)	Time 2 Median IVBA (%)	Time 3 Median IVBA (%)	Time 4 Median IVBA (%)	H statistic	p-value
Control Soil	3	87.47	101.1	97.66	97.18	9.462	0.02374
Unheated Biochar	3	85.10	99.37	95.21	94.62	9.462	0.02374
Heated Biochar	3	85.69	99.94	94.83	94.16	9.359	0.02488

Table 3-2. Dunn's post hoc test results for changes in Pb in-vitro bioaccessibility across sampling times (N=3).

Treatment	Timepoint comparison	z-statistic	p-value
Control Soil	Time 1 - Time 2	3.057	0.002235
	Time 1 - Time 3	1.698	0.08943
	Time 1 - Time 4	1.359	0.1742
	Time 2 - Time 3	1.359	0.1742
	Time 2 - Time 4	1.698	0.08943
	Time 3 - Time 4	0.3397	0.7341
Unheated Biochar	Time 1 - Time 2	3.057	0.002235
	Time 1 - Time 3	1.698	0.08943
	Time 1 - Time 4	1.359	0.1742
	Time 2 - Time 3	1.359	0.1742
	Time 2 - Time 4	1.698	0.08943
	Time 3 - Time 4	0.3397	0.7341
Heated Biochar	Time 1 - Time 2	3.057	0.002235
	Time 1 - Time 3	1.472	0.1410
	Time 1 - Time 4	1.585	0.1129
	Time 2 - Time 3	1.585	0.1129
	Time 2 - Time 4	1.472	0.1410
	Time 3 - Time 4	0.1132	0.9099

Because the data from 8 and 13 weeks (times t3 and t4 in Figure 3-1 panels A-C) show all samples remaining between about 93% and 98% bioaccessibility, we chose to investigate differences in Pb IVBA between treatments using only the last two timepoints. The Kruskal-Wallis test was used to test the null hypothesis that the median Pb IVBA values for each treatment were equal (Table 3-3). The p-value was 0.003889, indicating that at the 5% significance level, the three medians were not equal. Dunn's post-hoc test was conducted to determine which medians differed (Table 3-4). At the 5% significance level, median Pb IVBA was significantly higher in the control soil than in either the unheated biochar treatment ($p = 0.0110$) or the heated biochar treatment ($p = 0.001711$). However, the biochar treatments did not have significantly different median Pb IVBA values when compared to each other ($p = 0.5520$).

Table 3-3. Kruskal-Wallis test results for comparing median Pb in-vitro bioaccessibility (IVBA) in soil treatments at 8- and 13-week sampling times (degrees of freedom = 2). The H-statistic was 11.10 and the p-value was 0.003889.

Treatment	N	Median IVBA (%)
Control Soil	6	97.29
Unheated Biochar	6	94.95
Heated Biochar	6	94.49

Table 3-4. Dunn's post hoc test results for median Pb in-vitro bioaccessibility (IVBA) in soil treatments at 8- and 13-week sampling times (N=6).

Treatment comparison	z-statistic	p-value
Control soil – Unheated biochar	2.541	0.0110
Control soil – Heated biochar	3.136	0.001711
Unheated biochar – Heated biochar	0.5948	0.5520

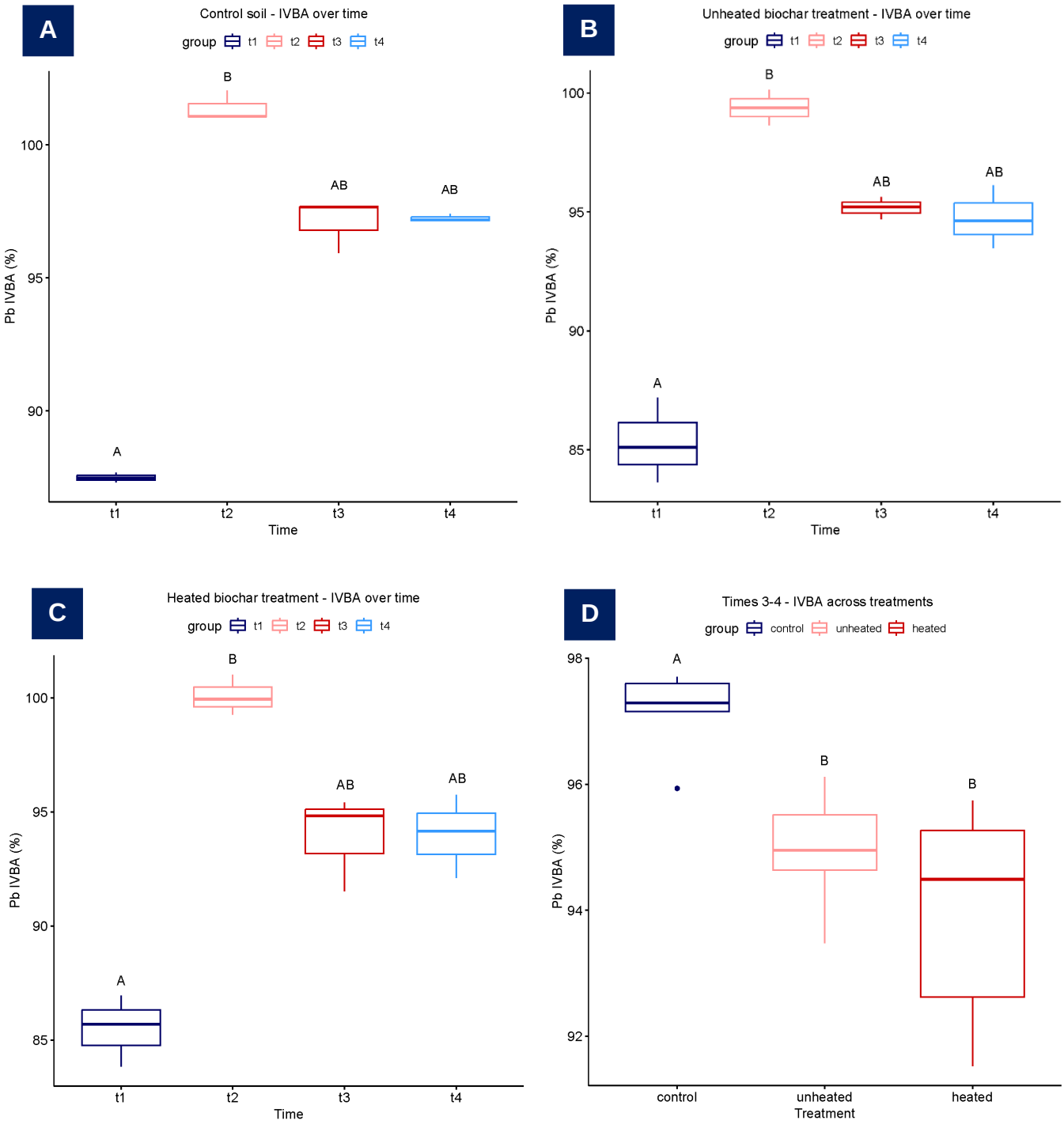

Figure 3-1. Boxplots of Pb in-vitro bioaccessibility (IVBA) for a trial experiment comparing soils treated with unheated and heated biochar. Compact letter displays show significant differences at the 5% level using the Kruskal-Wallis test and Dunn's post hoc test. (A) Changes in Pb IVBA across time in the control soil (n=3). (B) Changes in Pb IVBA across time in the soil amended with 5% w/w unheated biochar (n=3). (C) Changes in Pb IVBA across time in the soil amended with 5% w/w heated biochar (n=3). (D) Changes in Pb IVBA across treatments for the 8- and 13-week timepoints only (n=6).

Discussion

The biochar pH lowered from 10.26 to 8.79, supporting the conclusion that heating in air increases acidic surface groups on biochar surfaces. With heating, the biochar surface area also increased by 31.1%, while pore volume increased 48.0%. These changes indicate that heated biochar might have increased adsorption of Pb and therefore could reduce bioaccessible Pb in soil.

Soil pH was not significantly lowered across time and treatment, so the initial increase in bioaccessible Pb (Figure 3-1 panels A-C) was not likely due to pH-dependent changes in Pb solubility. Instead, the increase may be due to factors such as localized anaerobic conditions releasing Pb from iron oxides, or an initial increase in microbial activity breaking down insoluble organometallic complexes (the effects of soil moisture are explored further in Experiment 3). Although significantly lower Pb IVBA ($p < 0.05$) was identified in timepoints 3-4 in biochar treatments as compared to the control soil (Figure 3-1 panel D), this difference may or may not be of practical significance in the field.

Conclusions

Heat treatment in air decreased pH and increased the surface area and pore volume of biochar, suggesting potentially higher reactivity of the treated material. Non-parametric tests showed that both unheated and heated biochar treatments significantly reduced median Pb bioaccessibility after 8 weeks ($p < 0.05$). Heated biochar did not show a statistically significant improvement over unheated biochar in lowering Pb bioaccessibility. To further investigate these results, we continued with a larger-scale experiment using two different contaminated soils, biochar heated for different times, and a longer timeframe.

Experiment 2: Exploration of the effects of heated biochar on soil Pb bioaccessibility

Objective

After completing trial work with Philadelphia soil (≈500 mg kg^{-1} Pb; 5% biochar) in Experiment 1, we redesigned the study to better reflect practical remediation constraints and to probe early-time dynamics. Specifically, we (i) reduced the biochar dose to improve remediation cost, (ii) expanded thermal treatments to include 1, 3, and 4 h at 300°C, (iii) tested two Pb contamination levels (Low and High) to bracket common regulatory thresholds, (iv) shortened the incubation to 2 months but added more frequent sampling to resolve short-term changes, and (v) held similar initial moisture but did not maintain moisture thereafter, allowing soils to dry naturally over time. Together, these modifications were intended to evaluate whether lower-dose, thermally modified biochars can meaningfully alter Pb IVBA under field-leaning moisture regimes and across relevant concentration ranges. Soil was sourced from another location as a larger quantity was needed than was collected for Experiment 1.

Methods

Soil samples were taken in 2024 along the drip line of a row home located in Lancaster, PA, by Darren Parmer, Housing Intervention Manager for the Green & Healthy Homes Initiative. The size of the draw was 0.76 m by 6.71 m on the dripline of the gable end side of the house facing east.

The soil texture was classified following Gee & Bauder, 1986. The percent sand was determined by wet sieving the soil to 0.075 mm and weighing the sand following the hydrometer measurements (Gee & Or, 2018).

After drying at 105°C for two hours, the percent organic matter was determined using loss on ignition (Schulte & Hoskins, 2011). Three replicates were run and averaged for a final percent OM.

The soil Pb content was approximately measured using portable XRF (Vanta Element, Geochem) to be 2948 mg kg^{-1}. Two dilutions were then prepared using uncontaminated soil. The first dilution to ~200 mg kg^{-1} Pb (referred to hereafter as "Low Pb" soil) was made using 2.8 kg of Morrison soil mixed with 0.7 kg of the contaminated soil. The second dilution to ~600 mg kg^{-1} Pb (referred to hereafter as "High Pb" soil) used 3.267 kg Morrison soil and 0.233 kg contaminated soil. Samples of the soils were sieved to < 150 µm (as specified in EPA Method 1340) before sending to Agricultural Analytical Services Laboratory for EPA Method 3050B total Pb extraction followed by EPA Method 6010 ICP analysis (US EPA, 1996a, 1996b). The texture class and percent organic matter for each dilution were determined following the same procedures as described above.

Texture class and organic matter of the diluted soils were determined as above. Gravimetric field capacity was estimated by saturating air-dried (< 2 mm) soil in metal rings lined with cheesecloth, allowing 24 hours of saturation and 48 hours of drainage at room temperature, then oven-drying at 105°C to constant weight.

Wood chip biochar was again sourced from Metzler biochar but heated in larger batches as detailed in Chapter 3. Biochar was heated to 300°C for one-, two-, three-, and four-hour treatments. Biochar pH measurements were taken using the procedure recommended by the International Biochar Initiative (Rajkovich et al., 2012), and surface properties were characterized by IR spectroscopy and BET/FTR analyses as detailed in Chapter 2.

We chose the 1-, 3-, and 4-hour heated biochars for use in our experiment as these biochars showed large differences in pH and functional groups as compared to the unheated sample. 2-hour heated biochar was not used as it did not appear to be significantly different from 3-hour heated biochar.

For both contaminated soil mixtures, we set up the following conditions in 250-mL Nalgene bottles with 3 replicates each:

1. Unamended soil mixture
2. Soil mixture with 2% by mass unheated biochar

3. Soil mixture with 2% by mass 1-hour heated biochar
4. Soil mixture with 2% by mass 3-hour heated biochar
5. Soil mixture with 2% by mass 4-hour heated biochar.

Subsamples of each soil were taken for measuring total Pb: digestion by EPA method 3050B followed by ICP-OES testing using EPA Method 6010B. The total Pb measurements were averaged and used in calculating in-vitro bioaccessible (IVBA) Pb. One outlier with an unusually high total Pb (Grubb's outlier test p-value < 0.001) was removed from the Low Pb dataset.

The soils were wetted to approximately 38% moisture by mass (slightly lower than in Experiment 1 to account for lower organic matter content in the new soils) and each container was covered with perforated parafilm. Water was not added following the initial moistening. At the following timepoints, 25 g of soil was removed and dried at 35°C:

- T1: 1 day
- T2: 3 days
- T3: 1 week
- T4: 2 weeks
- T5: 1 month
- T6: 2 months.

A portion of each sample was then sieved to obtain 1 g of the < 150 μm fraction required for the EPA Method 1340 in-vitro bioaccessible Pb assay (2017 revision) (US EPA, 2017). The assay was carried out on the sieved samples and resulting solutions were sent to Penn State University's Agricultural Analytical Services Laboratory for ICP analysis (EPA Method 6010B) (US EPA, 1996b). For quality control, NIST soil standard 2711a was extracted and tested with each batch of samples; in all cases, its resulting IVBA was within the acceptable range listed in the EPA Method 1340 procedure.

Pb IVBA was calculated using the following formula: (Extracted Pb*100)/(Total Pb * Mass of Sample). Nonparametric statistical analyses (Kruskal-Wallis and Dunn's tests) were used, and statistical significance was determined using $\alpha = 0.05$.

Results

The hydrometer analysis showed a loam texture for the original soil, with the three LOI replicates giving an average of 6.15% organic matter. The average total Pb measurement of the Low Pb mixture was 259.84 mg kg^{-1} Pb, while that of the High Pb mixture was 721.48 mg kg^{-1} Pb. Both diluted soils were classified as sandy loams. For the Low Pb soil, three replicates averaged to 1.73% organic matter, and for the High Pb soil, three replicates averaged to 2.29% organic matter. Low Pb soil had an approximate gravimetric field capacity of 23.64%, while that of the High Pb soil was 23.24%.

In the low Pb soil, across all timepoints no significant differences were seen between treatments (Kruskal-Wallis p-value > 0.05). In the high Pb soil, significant differences between treatments were seen only in Time 1 (one day; H-statistic = 9.633 and p = 0.0471) and Time 3 (one week; H-statistic = 9.767 and p = 0.0445), so Dunn's post hoc test was run on those data (Tables 3-5 and 3-6). At Time 1, median IVBA Pb in soil treated with biochar heated for either 1 or 4 hours (88.07% and 90.83% IVBA, respectively) was significantly higher than in the control soil (82.96% IVBA; see Figure 3-2 panel A). At Time 3, median IVBA Pb in soil treated with unheated biochar or 1 hour-heated biochar (97.61% and 97.47% IVBA, respectively) was higher than in the control soil (86.45%; see Figure 3-2 panel B).

Table 3-5. Dunn's post hoc test results for comparing median Pb in-vitro bioaccessibility (IVBA) in high Pb soil treatments at Time 1 (one day of incubation).

Treatment comparison	z-statistic	p-value
Control – Unheated	1.643	0.1003
Control – Heated 1 hour	2.282	0.02248
Control – Heated 3 hour	1.369	0.1709
Control – Heated 4 hour	2.921	0.003487
Unheated – Heated 1 hour	0.6390	0.5228
Unheated – Heated 3 hour	0.2739	0.7842
Unheated – Heated 4 hour	1.2780	0.2012
Heated 1 hour – Heated 3 hour	0.9129	0.3613
Heated 1 hour – Heated 4 hour	0.6390	0.5228
Heated 3 hour – Heated 4 hour	1.552	0.1207

Table 3-6. Dunn's post hoc test results for comparing median Pb in-vitro bioaccessibility (IVBA) in high Pb soil treatments at Time 3 (one week of incubation).

Treatment comparison	z-statistic	p-value
Control – Unheated	2.739	0.006170
Control – Heated 1 hour	2.373	0.01762
Control – Heated 3 hour	1.004	0.3153
Control – Heated 4 hour	1.187	0.2353
Unheated – Heated 1 hour	0.3651	0.7150
Unheated – Heated 3 hour	1.734	0.08284
Unheated – Heated 4 hour	1.552	0.1207
Heated 1 hour – Heated 3 hour	1.369	0.1709
Heated 1 hour – Heated 4 hour	1.187	0.2353
Heated 3 hour – Heated 4 hour	0.1826	0.8551

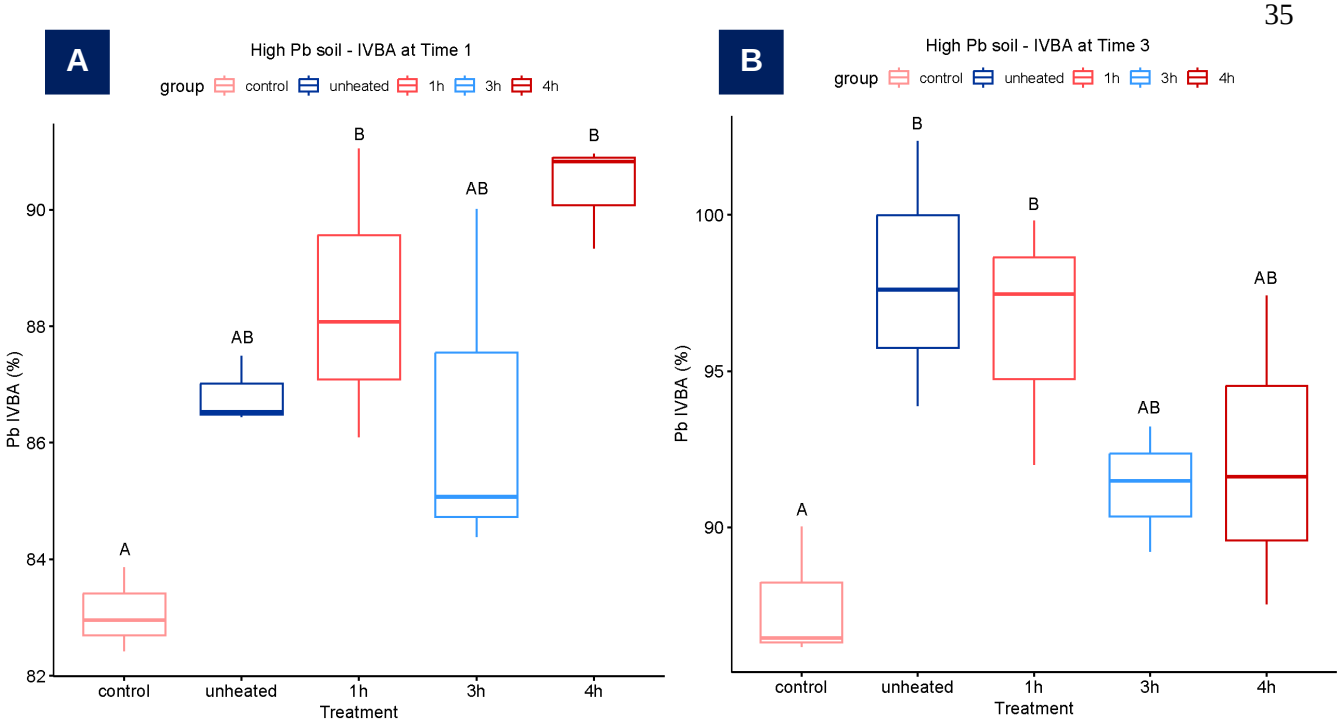

Figure 3-2. Boxplots of Pb in-vitro bioaccessibility (IVBA) for the high Pb soil treated with unheated and heated biochar at timepoints 1 (one day; panel A) and 3 (one week; panel B). Compact letter displays show significant differences at the 5% level using the Kruskal-Wallis test and Dunn's post hoc test (n=3). At time 1, Pb IVBA was lower in the control (unamended) soil compared to the soil amended with biochar heated for either 1 or 4 hours. At time 3, the control soil had lower Pb IVBA than soils amended with unheated biochar or 1 hour-heated biochar.

Looking at individual treatments over time, the Low Pb soil again did not show any significant variation (Kruskal-Wallis p-value > 0.05). In high Pb soil, unheated biochar, 3-hour heated biochar, and 4-hour heated biochar treatments showed variation over time, with Kruskal-Wallis tests giving H-statistics of 13.09, 13.68, and 14.05, and p-values of 0.0225, 0.0178, and 0.0153, respectively. Dunn's post hoc test was conducted on these groups (Tables 3-7, 3-8, and 3-9).

Table 3-7. Dunn's post hoc test results for comparing median Pb in-vitro bioaccessibility (IVBA) in high Pb soil treated with unheated biochar over time.

Timepoint comparison	z-statistic	p-value
1 – 2	1.835	0.06646
1 – 3	2.141	0.03226
1 – 4	0.6882	0.4913
1 – 5	1.071	0.2843
1 – 6	1.835	0.06646
2 – 3	0.3059	0.7597
2 – 4	2.524	0.01162
2 – 5	0.7647	0.4444
2 – 6	0	1
3 – 4	2.829	0.004663
3 – 5	1.071	0.2843
3 – 6	0.3059	0.7597
4 – 5	1.7589	0.07860
4 – 6	2.524	0.01162
5 – 6	0.7647	0.4444

Table 3-8. Dunn's post hoc test results for comparing median Pb in-vitro bioaccessibility (IVBA) in high Pb soil treated with 3-hour heated biochar over time.

Timepoint comparison	z-statistic	p-value
1 – 2	2.141	0.03226
1 – 3	0.8412	0.4002
1 – 4	0.6882	0.4913
1 – 5	2.141	0.03226
1 – 6	3.135	0.001717
2 – 3	1.300	0.1936
2 – 4	1.453	0.1462
2 – 5	0	1
2 – 6	0.9941	0.3202
3 – 4	0.1529	0.8784
3 – 5	1.300	0.1936
3 – 6	2.294	0.02178
4 – 5	1.453	0.1462
4 – 6	2.447	0.01440
5 – 6	0.9941	0.3202

Table 3-9. Dunn's post hoc test results for comparing median Pb in-vitro bioaccessibility (IVBA) in high Pb soil treated with 4-hour heated biochar over time.

Timepoint comparison	z-statistic	p-value
1 – 2	2.524	0.01162
1 – 3	0.4588	0.6464
1 – 4	0.8412	0.4002
1 – 5	1.224	0.2211
1 – 6	1.453	0.1462
2 – 3	2.065	0.03895
2 – 4	3.365	0.0007661
2 – 5	1.300	0.1936
2 – 6	1.071	0.2843
3 – 4	1.300	0.1936
3 – 5	0.7647	0.4444
3 – 6	0.9941	0.3202
4 – 5	2.065	0.03895
4 – 6	2.294	0.02178
5 – 6	0.2294	0.8186

In the unheated biochar treatment, Pb IVBA increased from Time 1 to Time 3, decreased at Time 4, and finally increased at Time 6 (Figure 3-3). A similar trend was observed in both 3- and 4-hour heated biochar treatments (Figures 3-4 and 3-5). In all three cases, IVBA tended to initially spike and then decrease before increasing again, similar to the pattern observed in Experiment 1 (Figure 3-1 panels A-C).

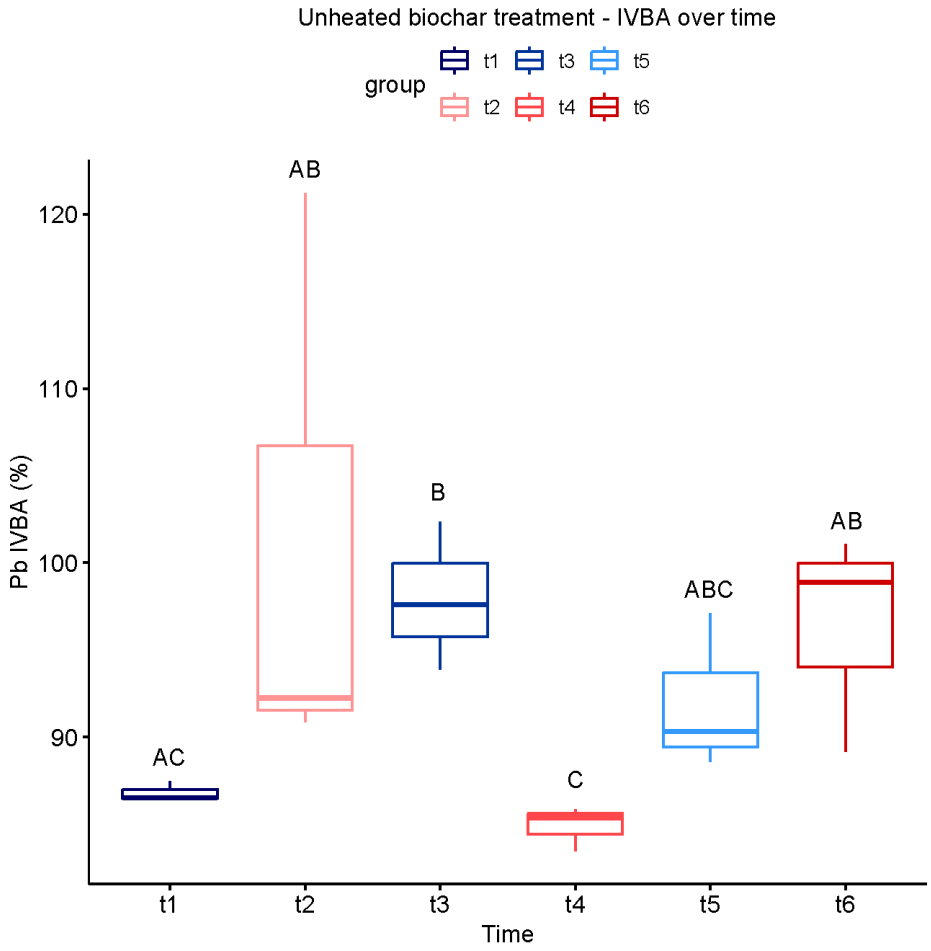

Figure 3-3. Boxplot of Pb in-vitro bioaccessibility (IVBA) for the high Pb soil treated with unheated biochar over time. Compact letter displays show significant differences at the 5% level using the Kruskal-Wallis test and Dunn's post hoc test (n=3). Median Pb IVBA increased from Time 1 to Time 3, decreased at Time 4, and finally increased again at Time 6.

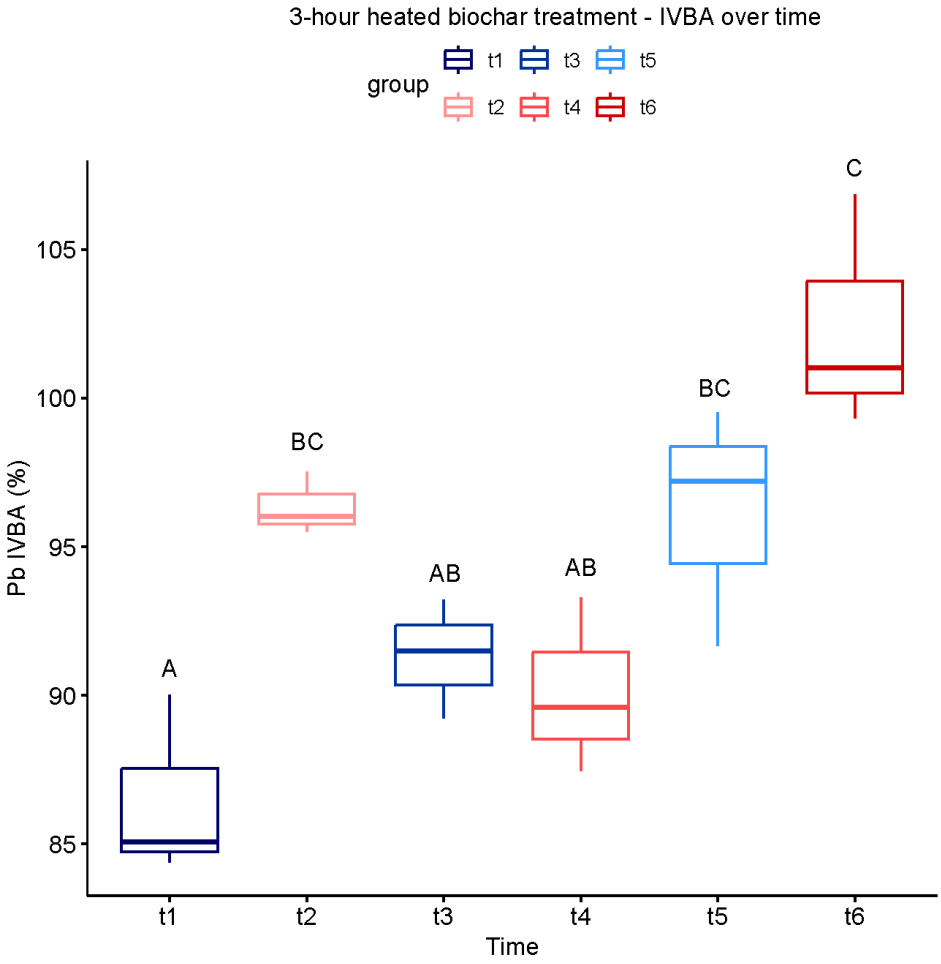

Figure 3-4. Boxplot of Pb in-vitro bioaccessibility (IVBA) for the high Pb soil treated with 3-hour heated biochar over time. Compact letter displays show significant differences at the 5% level using the Kruskal-Wallis test and Dunn's post hoc test (n=3). Median Pb IVBA increased from Time 1 to Time 2 and increased again at Time 6.

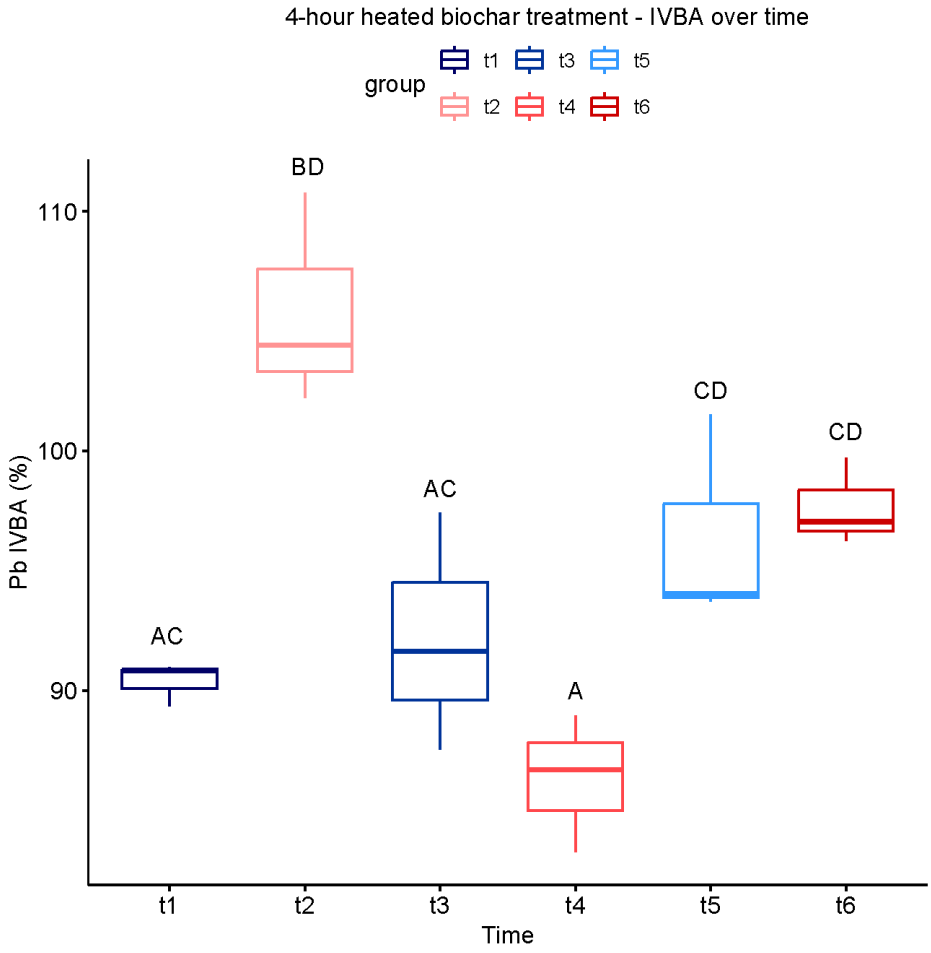

Figure 3-5. Boxplot of Pb in-vitro bioaccessibility (IVBA) for the high Pb soil treated with 4-hour heated biochar over time. Compact letter displays show significant differences at the 5% level using the Kruskal-Wallis test and Dunn's post hoc test (n=3). Median Pb IVBA increased from Time 1 to Time 2, decreased at Times 3 and 4, and finally increased again at Times 5 and 6.

Discussion

In the Low Pb soil, we did not see any significant differences in Pb IVBA across treatments or timepoints. In the High Pb soil, significant differences between treatments were only seen at timepoints 1 and 3 (one day and one week). At time 1, median Pb IVBA was lower in the control soil than in soil amended with biochar heated for either 1 or 4 hours. At time 3, the control soil had lower median Pb IVBA than soils amended with unheated biochar or 1 hour-heated biochar.

The lack of IVBA reduction in the Low Pb soil could be due to Pb being already bound by reactive particles in the soil such as clays or organic ligands. With the majority of timepoints in the High Pb soil not showing significant differences in IVBA across treatments, we conclude that the biochar reactivity investigated in Chapter 2 may not translate to Pb exposure-reducing effects in the soil environment. In fact, in the two cases where significant differences were seen, unamended soil had lower IVBA than certain amended soils. It is important to note that a biochar that is highly reactive in pure water can behave differently in soil, where competing reactive surfaces—organic matter, clay minerals, and Fe/Mn oxides—are abundant. These native sorbents and dissolved ligands compete with biochar for Pb, and ash-derived cations or DOC from the char can further shift equilibria. Another important parameter is soil moisture, which strongly influences the soil redox environment by shifting conditions between water-saturated (reducing) and unsaturated (oxic) states (Plunkett et al., 2022). Thus, properties that enhance reactivity in simplified systems may not translate to net Pb scavenging in soil matrices and may even increase Pb extractability in EPA Method 1340.

Over time in the High Pb soil, we observed a zig-zag pattern similar to what was seen in Experiment 1: Pb IVBA initially increased, decreased, and then increased again. While only significant in three of the five treatments, overall, the pattern does appear to be consistent with time-dependent processes (e.g., shifts in soil chemistry or redistribution between solid and solution phases) that might modulate Pb bioaccessibility irrespective of treatment.

In summary, the results indicate that wood-chip biochar at 2% (unheated or heated 1-4 h at 300°C) is not an effective immobilization amendment for this soil. Site-specific screening of alternatives that demonstrably lower IVBA (e.g., phosphate/apatite or Fe/Mn-oxide–rich amendments) could yield better results, with verification at both low and high Pb loadings using the same EPA Method 1340 protocol. Further, Pb IVBA appears to fluctuate significantly over time, warranting further investigation.

Conclusions

After our initial trial experiment showed a significant, albeit small, lowering of Pb IVBA in 5% (w/w) biochar-amended soil, we redesigned the study to better reflect practical remediation constraints and to probe early-time dynamics. Specifically, we reduced biochar dose, expanded thermal biochar treatments to include 1, 3, and 4 h at 300°C, tested two Pb contamination levels (low and high), and added more frequent sampling to resolve short-term changes. Fluctuations over time were observed, likely corresponding to background effects of soil conditions on the behavior of Pb species. Significant differences in treatments were only seen the high Pb soil at time 1 (one day) and time 3 (one week), where some biochar treatments raised Pb IVBA rather than lowering it as hypothesized. In conclusion, this variety of wood-chip biochar at 2% (unheated or heated 1-4 h at 300°C) did not prove to be an effective immobilization amendment for these soil conditions.

Our results highlight the importance of careful testing of individual biochar types in specific soil conditions prior to recommendation of use in the field. Additionally, trusted and low-cost methods of creating safe gardening environments—such as practicing good hygiene and using raised beds filled with clean soil—cannot be replaced by amendments.

Experiment 3: Effects of soil moisture on Pb bioaccessibility

Objective

The previous two experiments both used high moisture contents (40% and 38% by mass) and showed significant variation in Pb bioaccessibility over time. These findings raised the question of how soil moisture might affect biochar amendments and extractable Pb. While researching biochar effects on bioaccessible Pb in wetland soils, Plunkett et al. found that *in situ* redox conditions of samples from saturated environments influence Pb bioaccessibility (Plunkett et al., 2022). This experiment aimed to

answer the question of how soil moisture may have affected the previous two experiments' results by comparing Pb IVBA from control and biochar-amended soil below, at, and above field capacity.

Methods

The High Pb soil mixture (721.48 mg Pb kg^{-1}) from Experiment 2 was used in this experiment. The soil was incubated with and without the addition of 2% by mass unheated Metzler wood chip biochar at three different moisture levels: low (10% gravimetric moisture content—below saturation), medium (23% gravimetric moisture content—near field capacity), and high (46.9% gravimetric moisture content—at saturation, calculated from soil bulk density). Each sample of 18 g oven-dry soil was brought to the appropriate mass by the addition of DI water. Each condition was replicated four times.

Following a 2-day incubation, samples were freeze-dried in an attempt to preserve redox-sensitive species prior to extraction (Furman et al., 2007). Bioaccessible Pb was then extracted following EPA Method 1340. The extraction solutions were measured with a benchtop EDXRF calibrated by regression analysis against ICP-OES, as detailed in Chapter 4.

Results

In the control soil, Pb IVBA decreased steadily from 104.19 ± 2.95% to 72.95 ± 3.43% with increasing soil moisture content (Figure 3-6). In the amended soil, Pb IVBA peaked with medium moisture content (114.97 ± 4.82%) and was lowest with high moisture content (85.21 ± 1.44%).

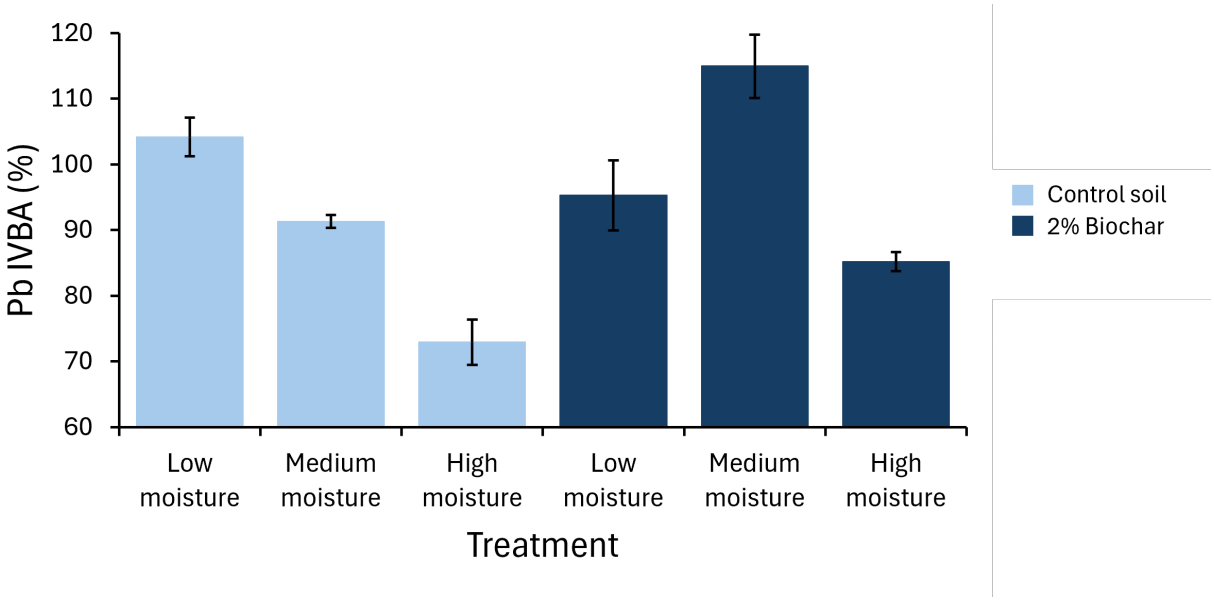

Figure 3-6. Bar chart showing changes in Pb in-vitro bioaccessibility (IVBA) after two days under varying moisture contents in a contaminated soil (Pb 721.48 mg kg^{-1}) with and without 2% unheated biochar added. Error bars show standard error among 4 replicates.

Discussion

Pb in-vitro bioaccessibility (IVBA) in the control soil showed a steady decrease as gravimetric moisture increased, from 104.19 ± 2.95% at low moisture (~10%) to 91.31 ± 0.98% at medium moisture (~23%, near field capacity) and ~73.95 ± 3.43% at high moisture (~47%, near saturation) (n = 4). This monotonic decrease could be explained with a shift from oxic toward suboxic/anaerobic conditions at higher water contents, which (1) can promote microbial sulfate reduction and sulfide production, driving precipitation of sparingly soluble PbS that may be less extractable by EPA Method 1340; (2) tends to raise pH/alkalinity during reductive processes, favoring Pb sorption and formation of carbonate/hydroxyl-carbonate solids; and (3) alters Fe/Mn redox cycling, generating Fe(II) phases and FeS surfaces that (re)sequester dissolved Pb (Pignatello et al., 2024).

In contrast, the 2% biochar treatment showed a hump-shaped response: IVBA increased from 95.32 ± 5.34% (low moisture) to 114.97 ± 4.82% (medium moisture) and then dropped to 85.21 ± 1.44%

(high moisture), converging with the control at near-saturation. The mid-moisture peak likely reflects conditions optimal for microbial activity and solute diffusion that enhance desorption/complexation (e.g., higher DOC), whereas at high moisture the same mechanisms (1–3) dominate, lowering IVBA in both treatments. Specifically, at intermediate moisture (≈ field capacity), soils have the best balance of water and oxygen for microbes and solute transport, which can temporarily raise Pb IVBA. First, aerobic microbial activity and extracellular enzyme diffusion peak near field capacity, accelerating decomposition and releasing dissolved organic carbon (DOC) (Birch, 1958; Skopp et al., 1990). Second, DOC—especially low-molecular-mass acids and fulvic/humic ligands—complexes Pb in solution and can compete with mineral and organic sorption sites, shifting Pb from surface-bound to dissolved/ligand-bound forms (McBride et al., 1997; Sauvé et al., 1998; Tipping, 2002). Third, higher moisture improves diffusive transport, helping DOC and inorganic ligands reach sorption domains and mobilize surface-associated Pb before stronger reducing conditions develop at near-saturation; once pores become water-filled and O_2 is limited, sulfide formation and Fe(II)/FeS surfaces re-immobilize Pb, so IVBA drops again.

The contrast between the control soil and the biochar-amended soil can be explained by fundamental redox processes. Biochar contains redox-active carbon matrices with measurable electron-donor capacity (EDC) and electron-acceptor capacity (EAC)—quantities (meq g^{-1}) describing how much charge the material can reversibly donate or accept (Klüpfel et al., 2014; T. Sun et al., 2017; Y. Yuan et al., 2017). Quinone/hydroquinone moieties, aromatic sheets, and persistent free radicals in biochar act as electron-storage and shuttle sites, enabling rapid electron transfer to or from surrounding minerals, solutes, and microorganisms (Klüpfel et al., 2014; T. Sun et al., 2017). Through these coupled half-reactions, biochar can reduce electron acceptors such as Fe(III), Mn(IV), or Cr(VI), or oxidize reduced species when oxygen or nitrate is present, thereby altering soil redox potential (Eh) and the speciation of metals such as Pb (Husson, 2013; Stumm & Morgan, 1996).

During these electron exchanges, reactive oxygen species (ROS) such as hydrogen peroxide (H_2O_2), superoxide (O_2^-), and hydroxyl radicals (•OH) can form. These short-lived oxidants originate when O_2 accepts electrons supplied by biochar EDC, or when H_2O_2 decomposes on redox-active surfaces (Yuan et al., 2017). ROS can further transform Pb and Fe minerals, shifting Pb from more soluble to less soluble phases depending on moisture and redox status (Antić-Mladenović et al., 2017).

In our soils, the control (soil SOM only, no biochar) showed steadily lower Pb IVBA as moisture increased, consistent with decreasing Eh and precipitation of sulfide or carbonate phases under reducing conditions after nitrate and ferric iron depletion (Husson, 2013; Stumm & Morgan, 1996). By contrast, the biochar-amended soil had higher Pb IVBA at low to medium moisture, where its strong EDC and surface alkalinity favored transient Pb mobilization, but converged with the control at high moisture when strongly reducing conditions immobilized Pb. This behavior mirrors field evidence: Plunkett et al. (2022) found that biochar modestly lowered Pb bioaccessibility in upland soils but had little effect in periodically flooded soils where oxidation of Pb sulfides during drying nearly doubled bioaccessibility. Likewise, a meta-analysis of biochar aging shows that O-functionalization (↑EAC, ↓EDC) and microbial activity gradually reshape biochar's redox behavior and its control over metal solubility (Yuan et al., 2021).

Conclusions

Together, these findings show that biochar may act as a long-lived redox capacitor: it stores and releases electrons (high EDC/EAC), generates ROS, and buffers Eh. However, its impact on Pb mobility ultimately depends on the prevailing moisture-redox regime and on longer-term chemical and microbial aging.

Chapter 4

Assessing the Capability of Energy-Dispersive X-Ray Fluorescence Spectroscopy as an Alternative to ICP-OES for Pb Quantification in Liquid Environmental Samples

Introduction

Urban soil Pb contamination

Urban agriculture is increasingly promoted to enhance food security, foster community engagement, and support economic revitalization in underserved areas (Hanna & Oh, 2000; Horst et al., 2017). However, urban soils may be contaminated with heavy metals, particularly lead (Pb), which poses significant risks to human health (Landes et al., 2023).

Pb contamination typically originates from sources such as leaded gasoline, Pb-based paint, industrial emissions, and improper waste disposal (US EPA, 2013). Over time, Pb-containing pollutants have accumulated in surface soils, posing health risks when contaminated particles are inhaled or ingested (Landes et al., 2023). To address these risks, reliable testing methods are needed to assess the various forms and behaviors of Pb in soil. Reliable analytical methods are therefore essential to evaluate the different forms and environmental behaviors of Pb (Wharton, et al., 2012).

Solution-based extractions are widely employed to evaluate Pb mobility, bioaccessibility, and potential exposure pathways. This study focuses on three representative solution types: (1) EPA Method 1340 simulated gastric fluid extractions, which estimate the fraction of Pb soluble under stomach conditions (US EPA, 2017; Zia et al., 2011); (2) $Pb(NO_3)_2$ solutions, frequently used to spike soils and amendments for Pb sorption capacity assessment (Elbana et al., 2018; Li, Wu, et al., 2023; Masson, G. et al., 2025); and (3) Mehlich 3 extractions, a standard agronomic test for nutrients and trace metals that has also been used as a proxy for estimating bioaccessible Pb (Mehlich, 1984; Minca et al., 2013).

Each of these approaches provides insight into distinct environmental processes and informs remediation, soil management, and land reuse strategies. Traditionally, the analysis of such extracts relied on inductively coupled plasma-optical emissions spectroscopy (ICP-OES, hereafter ICP), an accurate but costly and resource-intensive analytical method. ICP operates by converting sample solutions into aerosols, which are then introduced into a plasma source. The analytes absorb energy from the plasma and are excited to higher electronic states. As the atoms return to their ground state, they emit at element-specific wavelengths that can be used for identification and quantification.

X-ray fluorescence (XRF) spectroscopy is a non-destructive technique for elemental analysis that provides concentrations of elements ranging from sodium to uranium. Samples can be prepared as liquids or powders (lower accuracy) and flattened pellets or fused beads (higher accuracy). X-rays directed at the sample eject inner-shell electrons; subsequent electronic transitions from higher orbitals release energy in the form of element-specific fluorescent X-rays. Because each element has a unique emission profile, XRF allows for both qualitative identification and quantitative analysis of metals. XRF on solid samples has often been compared to ICP on analytes extracted into solution, with XRF showing excellent performance (Chojnacka et al., 2018; Maliki, et al., 2017; Ramsey et al., 1995). However, in this work, we are interested in comparing the two techniques for analysis of liquid extractions, an aspect of XRF that remains understudied (Margui et al., 2022).

Limitations of ICP for routine testing

ICP is an EPA-approved and widely established method for quantifying elemental concentrations in environmental samples (Pyle et al., 1996). It is valued for its high sensitivity, precision, and ability to detect metal concentrations across a wide range of matrices. However, the widespread application of ICP in routine soil and water testing, particularly in under-resourced or field settings, is limited by several factors.

First, ICP instrumentation requires substantial capital investment (~$100,000) and incurs high operating costs (Thomas, 2016). In addition to high acquisition costs, ICP involves significant operating expenses, including the use of large volumes of argon gas (Wilbur, 2005). Ongoing maintenance and routine calibration with certified standards further add to the complexity and cost. Second, effective operation of ICP demands trained personnel with expertise in analytical chemistry and instrument management, limiting its availability to smaller laboratories and community-based environmental testing efforts. Finally, because ICP analyses are often centralized in specialized facilities, logistical delays can occur in sample transport and result turnaround, which is particularly problematic for time-sensitive decisions in field-based remediation projects.

These constraints highlight the need for simpler, faster, and more affordable alternatives for routine elemental analysis. In the context of Pb contamination in urban soils, the availability of rapid and accessible screening methods could significantly improve monitoring capacity and support timely public health protection.

XRF for environmental testing

X-ray fluorescence (XRF) spectroscopy is increasingly recognized as a practical alternative for elemental analysis, particularly in soil science, mining, and archaeology applications (Marguí et al., 2022). Traditionally applied to solid samples, XRF offers non-destructive, multi-element detection with minimal sample preparation. However, its application to liquid samples remains limited due to physical and technical challenges associated with liquid matrices.

One major hurdle is that fluorescent X-rays emitted by elements in aqueous solutions are significantly attenuated by the water matrix, reducing both sensitivity and reproducibility. Although sample preparation techniques such as pre-concentration or water removal can improve detection limits and signal-to-noise ratios (Moradi et al., 2015), these methods are often complex, time-consuming, and

costly. Furthermore, liquid samples can introduce measurement variability through evaporation, bubble formation, and sample heterogeneity (Marguí et al., 2014). Despite these challenges, XRF has important advantages. It requires minimal sample preparation, consumes no reagents or gases, and provides rapid results without the need for dilution. Most importantly, benchtop XRF units are relatively affordable (~$65,000 for a new, mid-range instrument), easy to operate, and require minimal maintenance (Marriott, 2025). These features make benchtop systems well-suited for use in community laboratories, field stations, and educational settings, though performance may vary depending on the specific model and type of XRF instrument used (e.g., energy-dispersive vs. wave-dispersive types).

Pb, a relatively heavy element with a high Lα line energy (10.549 keV), remains detectable in aqueous solutions using XRF, provided the instrument is properly configured. For example, recent advances let benchtop XRF instruments pair high-power X-ray tubes with large-area detectors and optimized excitation geometry, maximizing sensitivity while minimizing background ("Energy Dispersive X-Ray Fluorescence Spectrometer," 2023). These properties present opportunities for applying XRF to solution analyses traditionally restricted to ICP-based methods, including in vitro bioaccessibility assays, sorption studies, and nutrient extraction analyses.

Building on these developments and the fact that Pb is a heavy element with strong fluorescence, we hypothesize that, across the three chemically-distinct matrices evaluated here, XRF results will show strong linear correlation ($r^2 > 0.98$) with ICP-OES measurements, indicating that matrix effects do not introduce unacceptable analytical bias. If validated, this would broaden the utility of XRF to include Pb bioaccessibility assays and sorption studies.

Objective

The primary objective of this study is to evaluate the performance of energy-dispersive benchtop XRF in measuring lead concentrations in liquid environmental samples, with the goal of establishing XRF as a possible alternative to ICP for specific use cases.

To test this, we conducted regression comparisons of XRF and ICP measurements across multiple types of Pb-containing solutions commonly used in environmental research:

Regression 1: EPA Method 1340 *in vitro* bioaccessibility extracts (used to estimate human ingestion risk)

Regression 2: $Pb(NO_3)_2$ solutions used in experiments modeling soil contamination

Regression 3: Mehlich 3 extracts used for assessing plant-available nutrients and trace metal bioaccessibility in soil.

By comparing the XRF and ICP results for these sample types, we aim to determine the accuracy, reproducibility, and limitations of benchtop XRF for liquid analysis. Ultimately, we propose that XRF (when properly calibrated and applied) can serve as a cost-effective and accessible tool for lead monitoring in environmental and urban soil contexts, enabling more rapid decision-making in public health and remediation efforts.

Methods

Regression 1: EPA Method 1340 Pb extraction from soils

37 contaminated soil samples were collected from multiple locations in Philadelphia, PA, in 2022 (Dadio, S., 2024). Bioaccessible Pb extractions were performed following the EPA Method 1340 procedure: samples are sieved to < 250 µm (per the 2013 method revision) and digested for 1 hour at 37°C using a 0.4 M glycine solution acidified with HCl to a pH of 1.5 (US EPA, 2017). The solution was separated from soil solids using a 0.45 µm syringe filter and refrigerated at 4°C until analysis. For each batch of samples, NIST soil standard 2711a was extracted and tested as well for quality control purposes; in all cases, it was within the acceptable range listed in the EPA Method 1340 procedure.

Regression 2: $Pb(NO_3)_2$ solution for adsorption on biochar

30 solutions of varying concentrations of Pb were prepared using $Pb(NO_3)_2$ (ACS reagent-grade, ≥ 99.0%) dissolved in Type I water. A drop of reagent-grade concentrated nitric acid was used to acidify each solution to below pH 2. The approximate concentrations were made starting at 1 mg Pb L^{-1} and then in increments of 25 mg Pb L^{-1} (1, 25, 50, … , 700, 725 mg Pb L^{-1}).

Each solution was measured on XRF with water as the balance and a blank ASTM Type I water sample as the impurity. The working calibration range of Pb for the ICP was 0.025 to 100 mg L^{-1}, so the solutions were diluted by a factor of 10 prior to ICP analysis.

Regression 3: Mehlich 3 extracts of Pb-contaminated soils

A subset of soils previously characterized as part of the Northeast Coordinating Committee project NECC-1812 (Hamel et al., 2003) was used to assess Pb content and XRF response. These soils represent a range of management histories and physicochemical properties relevant to urban and agricultural contexts. For this dataset, air-dried soil passing a 2 mm sieve was extracted using Mehlich 3 method (Mehlich, 1984; Wolf and Beegle, 2011). Briefly, 20 ml of Mehlich 3 solution (0.2 *N* CH_3COOH + 0.25 *N* NH_4NO_3 + 0.015 *N* NH_4F + 0.013 *N* HNO_3 + 0.001 *M* EDTA) was added to 2 g of weighed soil in a 50 mL plastic beaker. Beakers were placed on a reciprocating shaker for 5 minutes at 180 oscillations per minute. The extracted solution was filtered using Advantech No. 1 filter paper and stored at 4°C.

ICP and XRF analysis

Pb concentrations in EPA Method 1340 and $Pb(NO_3)_2$ solutions were analyzed by ICP-OES (Varian 730-ES Axial ICP Spectrometer, now Agilent Technologies, Santa Clara, CA) following EPA Method 6010B. For Mehlich 3 solutions, quality assurance included analysis of an independent

calibration verification standard before sample measurement and a continuing calibration verification standard every 10 samples, and at the end of each run, with results required to be within 10% of expected values. A method blank and laboratory quality control sample were also run with each batch of 28 samples.

Analyses were performed on a Rigaku NEX CG II benchtop EDXRF spectrometer equipped with a Pd X-ray tube, a silicon drift detector, and a 15-position autosampler (referred to in this paper as benchtop, XRF) (“Energy Dispersive X-Ray Fluorescence Spectrometer,” 2023).

For each batch of extracted samples, a blank sample (either 0.4 M glycine, type I water, or Mehlich 3 extract, depending on the measured solution type) was tested first. This “background spectrum” was subtracted from subsequent sample measurements. We found that when many analytes were selected, interference increased, so Pb was selected as the only analyte. Additionally, to account for the matrix effects we used glycine as the “balance” in the software for EPA Method 1340, and water for both Pb-nitrate solutions and Mehlich 3 extracts. The “balance” setting allows the XRF software to quantify the detectable components in a sample while accounting for unmeasurable components (i.e., light elements).

Statistics

The “Statistical error” output on the Rigaku EDXRF instrument is the $\pm 1\sigma$ uncertainty from counting noise: the software integrates the element’s net peak (after background), where N is the photon counts collected ($\approx$ intensity I in cps/mA $\times$ live time t in s); the Poisson 1σ is $\sqrt{N}$, which is then propagated through the calibration and Fundamental Parameters model to give the uncertainty in mg L^{-1}.

Minitab software (Minitab, LLC, 2023) was used for regression analyses and checks of model assumptions. For each dataset, we assessed model assumptions including linearity, normality of residuals

(Anderson–Darling test), and homogeneity of variance (F-tests, Breusch–Pagan test). Where assumptions were violated (Mehlich 3 dataset), data were log–log transformed, and high-leverage points were evaluated prior to refitting the model. Regression outputs included the model equation, 95% confidence intervals for slope and intercept, coefficient of determination (r^2), root mean square error (RMSE), p-values, and residual plots. For EPA Method 1340 and Mehlich 3 data, model validation was conducted by randomly splitting the dataset into approximately 80% for training and 20% for validation. For the $Pb(NO_3)_2$ model, we separately mixed solutions of varying concentration for the validation set. The measured XRF values were entered into the regression equations to calculate predicted ICP values, which were then plotted against the corresponding measured ICP values, with predicted values on the x-axis and measured values on the y-axis.

Results and discussion

Precision of XRF measurements

The average values of statistical errors, limits of detection, and limits of quantification for each regression solution are shown in Table 4-1.

Table 4-1. Statistical error, detection limit, and quantification limit for Pb measurements by benchtop EDXRF across three solution types.

	Average value (mg L^{-1})			
Solution	Standard deviation	Statistical error	Detection limit	Quantification limit
EPA Method 1340	0.055	0.0856	0.170	0.509
$Pb(NO_3)_2$	1.501	0.8466	0.250	0.751
Mehlich 3	0.094	0.1566	0.236	0.709

EPA Method 1340 regression results and discussion

Checks of simple linear regression assumptions

For EPA Method 1340 extracts, the assumptions of simple linear regression (linearity, normality of residuals, and homogeneity of variance) were satisfied:

1. Scatterplots indicated a linear relationship between ICP and XRF values (see Figure 4-1).
2. Residuals versus fits plots showed a roughly horizontal band with random scatter, suggesting constant variance.
3. The Anderson-Darling test supported normality of residuals ($p = 0.201$), confirming normality at the 5% significance level.

Regression results

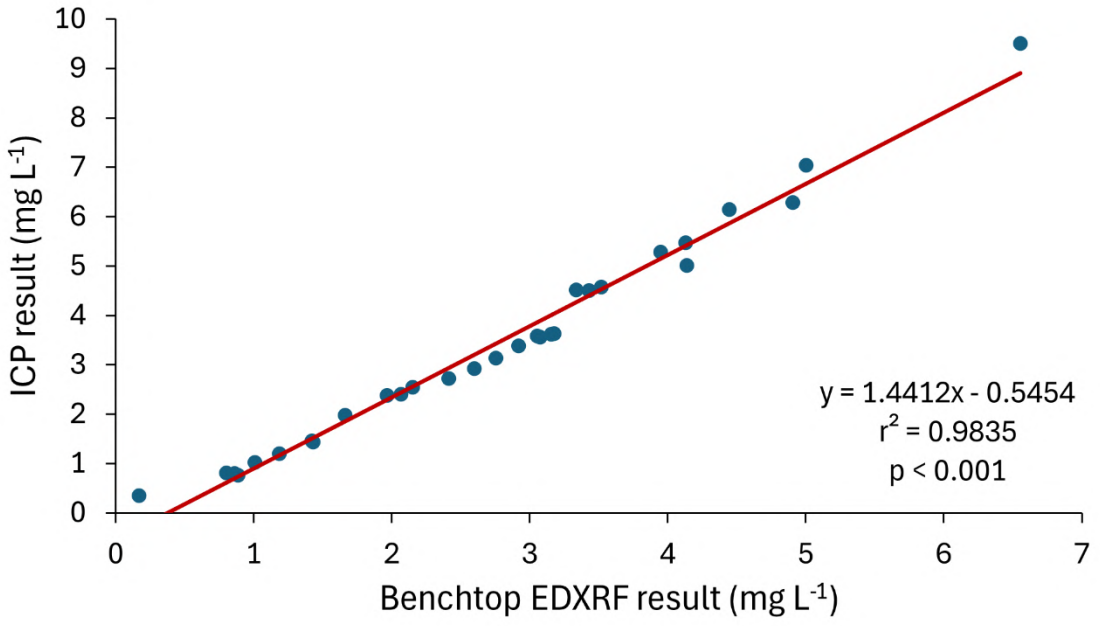

Figure 4-1. Linear regression scatterplot of benchtop EDXRF results (average of 3 measurements) and ICP results for Pb in EPA Method 1340 extracts. N = 30.

For EPA Method 1340 bioaccessible Pb extracts, the regression equation was:

$$ICP\ (mg\ L^{-1}) = -0.545 + 1.4412 \times XRF\ (mg\ L^{-1}).$$

The slope was 1.4412 with a 95% confidence interval of 1.369 to 1.513 and a p-value of < 0.001. The y-intercept was –0.548 with a 95% confidence interval of –0.770 to –0.320 and a p-value of < 0.001. The model's r^2 was 0.9835 with an overall p-value of < 0.001. The RMSE (root mean square error) was 0.2811.

Model validation results

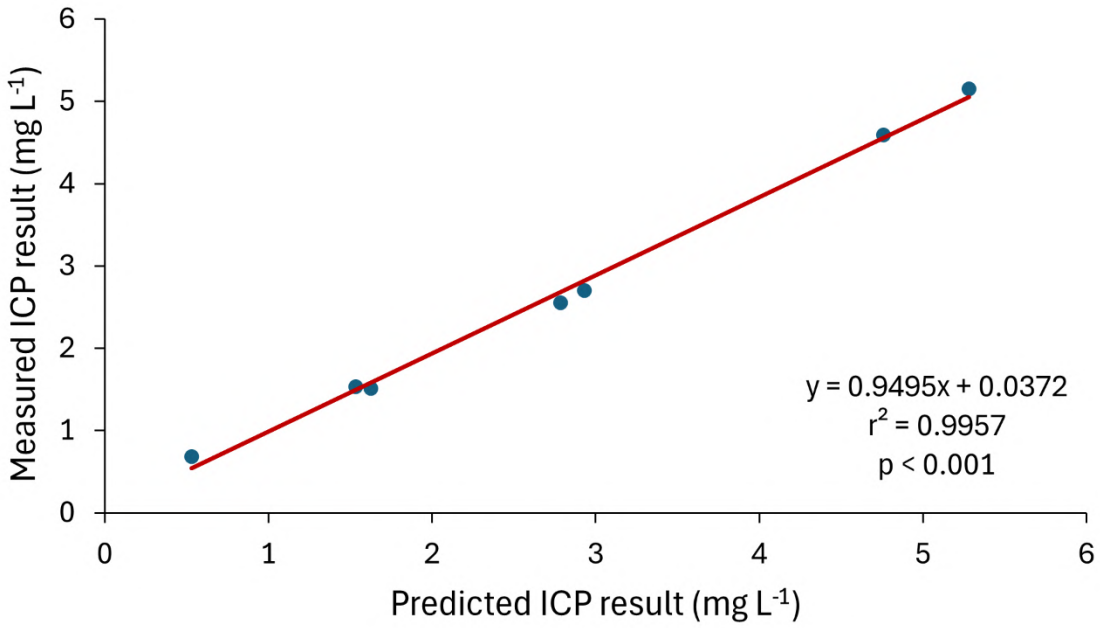

Figure 4-2. Linear regression scatterplot of the validation dataset for Pb measured in EPA Method 1340 extracts. The predicted ICP result was obtained using EDXRF measurements entered into the regression model built using the training dataset (Figure 4-1). N = 7.

The validation regression equation was:

$$ICP_M\ (mg\ L^{-1}) = 0.0372 + 0.9495 \times ICP_C\ (mg\ L^{-1})$$

where ICP_M is the measured ICP result and ICP_C is the expected ICP result calculated by entering the XRF result into the training regression equation (Figure 4-2).

The slope was 0.9495 with a 95% confidence interval of 0.8778 to 0.0212 and a p-value of < 0.001. The y-intercept was 0.0372 with a 95% confidence interval of -0.1929 to 0.2673 and a p-value of 0.695. This high p-value means that we cannot reject the null hypothesis that the y-intercept is equal to 0. The model's r^2 value was 0.9957 with an overall p-value of < 0.001. The RMSE was 0.1187 and the mean absolute error (MAE) was 0.0928.

Discussion

For EPA Method 1340 extracts, the simple linear regression slope was 1.4412 with an intercept of –0.545 (Figure 4-1). The training model slope is greater than unity, suggesting that XRF tends to underestimate Pb concentrations relative to ICP, particularly at higher concentrations. The negative intercept (-0.545) reflects a small baseline offset between the two methods. This systematic bias underscores the importance of calibration when using XRF as a substitute for ICP. The predictor (XRF result) explained 98.35% of the variance in ICP results ($R^2 = 0.9835$), which would indicate an excellent fit.

The validation model showed excellent performance ($r^2 = 0.9957$, $p < 0.001$), indicating strong predictive ability of the training regression (Figure 4-2). Despite this bias, the validation set showed a high r^2 and low p-value, demonstrating that XRF, when adjusted using the regression equation, could serve as a reliable proxy for estimating ICP-derived Pb concentrations. The MAE was low (0.0918 mg L^{-1}), showing high predictive accuracy. The RMSE of the validation set (0.2811 mg L^{-1}) was somewhat higher than that of the training set (0.1187 mg L^{-1}), which-might indicate slight overfitting. The RMSE value might indicate that this technique could be limited to experiments where precision of ± 0.2811 mg L^{-1} is acceptable.

$Pb(NO_3)_2$ regression results and discussion

Checks of simple linear regression assumptions

For the $Pb(NO_3)_2$ dataset, the assumptions of simple linear regression were satisfied. Scatterplots confirmed that the relationship between ICP and XRF measurements was linear across the concentration range (Figure 4-3). Examination of residuals versus fitted values showed mostly random scatter at higher predictor values, although a slight curvature at the lower end of the concentration range suggested the

possibility of heteroscedasticity. To evaluate this further, the residuals were divided into two groups (low vs. high predictor values), and tests for equality of variance were performed. Both Bonett's test ($p = 0.079$) and Levene's test ($p = 0.074$) failed to reject the null hypothesis of equal variances, indicating no evidence of heteroscedasticity at the 5% significance level. Results from the Breusch–Pagan test supported the same conclusion ($p = 0.2408$).

The Breusch–Pagan calculation was as follows: residuals squared were regressed against the predictor values, yielding a sum of squared errors (SSE) of 3991 and a regression sum of squares (SSR*) of 48,700. The resulting chi-square statistic was:

$$\chi^{2*} = \frac{\frac{SSR^*}{2}}{\left(\frac{SSE}{n}\right)^2} = \frac{\frac{48700}{2}}{\left(\frac{3991}{30}\right)^2} = 1.376$$

For chi squared = 1.376, the corresponding $p = 0.2408 > 0.05$, confirming homoscedasticity. $p = 0.2408 > 0.05$. The Anderson–Darling test for normality also indicated that residuals were approximately normal ($p=0.06$). Together, these results confirmed that the regression assumptions of linearity, normality, and constant variance were satisfied for the $Pb(NO_3)_2$ model.

Regression results

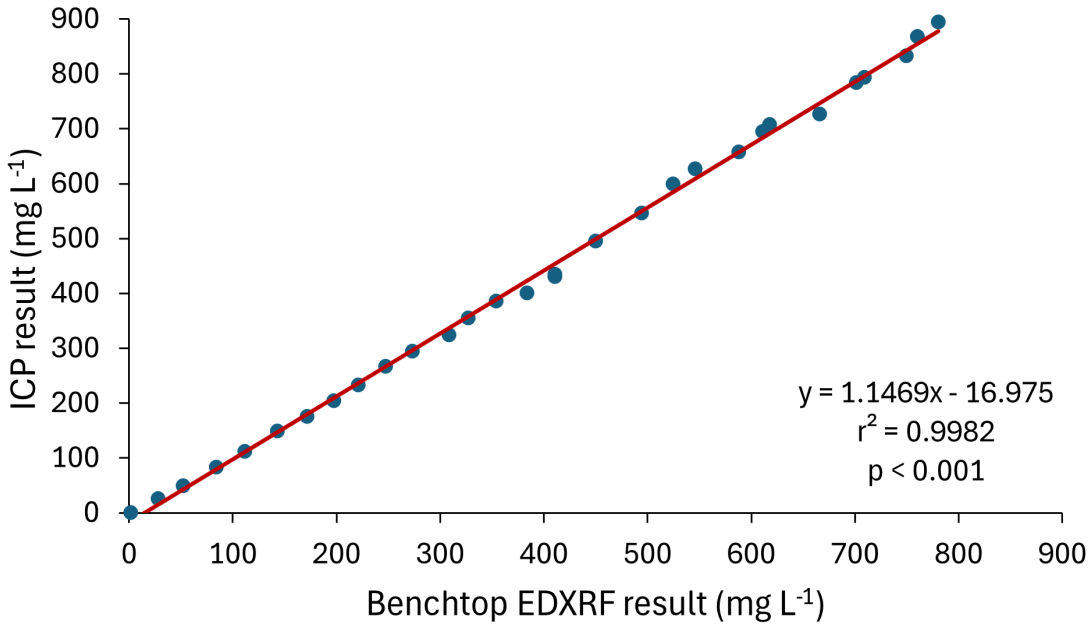

Figure 4-3. Linear regression scatterplot of benchtop EDXRF results (average of 3 measurements) and ICP results for Pb in aqueous $Pb(NO_3)_2$ solutions. N = 30.

For $Pb(NO_3)_2$ solutions, the regression equation was:

$$ICP\ (mg\ L^{-1}) = -16.98 + 1.147 \times XRF\ (mg\ L^{-1}).$$

The slope was 1.147 with a 95% confidence interval of 1.128 to 1.166 and a p-value of < 0.001. The y-intercept was –16.98 with a 95% confidence interval of –25.70 to –8.26) and a p-value of < 0.001. The model's r^2 value was 0.9982 with an overall p-value of < 0.001. The RMSE (root mean square error) was 11.96.

Model validation results

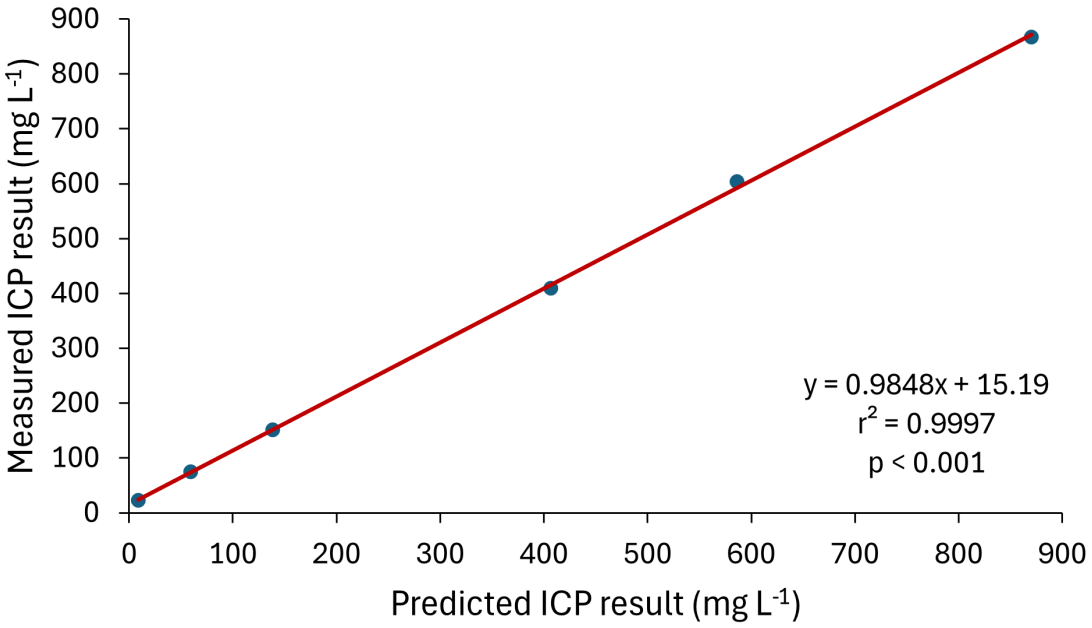

Figure 4-4. Linear regression scatterplot of the validation dataset for Pb measured in aqueous $Pb(NO_3)_2$ solutions. The predicted ICP result was obtained using EDXRF measurements entered into the regression model built using the training dataset (Figure 4-3). N = 6.

The validation regression equation was:

$$ICP_M\ (mg\ L^{-1}) = 15.19 + 0.9848 \times ICP_C\ (mg\ L^{-1})$$

where ICP_M is the measured ICP result and ICP_C is the expected ICP result calculated by entering the XRF result into the training regression equation (Figure 4-4).

The slope was 0.9848 with a 95% confidence interval of (0.9606, 1.009) and a p-value of < 0.001. The y-intercept was 15.19 with a 95% confidence interval of (4.003, 26.38) and a p-value of 0.020. The model's r^2 value was 99.97% with an overall p-value of < 0.001. The RMSE was 6.557 and the mean absolute error (MAE) was 4.0360.

Discussion

For $Pb(NO_3)_2$ solutions, the slope was 1.147 (95% CI: 1.128 to 1.166) with an intercept of –16.98 (95% CI: –25.70, to –8.26) (Figure 4-3). XRF results explained 99.82% of the variance in ICP results (r^2 = 0.9982) with a root mean square error (RMSE) of 11.96 mg L^{-1}.

The validation model showed excellent performance (^{2} = 0.9997, $p < 0.001$) and strong predictive ability of the training regression (Figure 4-4). The slope of the training model was greater than unity (1.147, Figure 4-3) suggesting that XRF may systematically underestimate Pb concentrations relative to ICP, particularly at higher levels. However, this slope is closer to 1 than the slope of the EPA Method 1340 model, so XRF may underestimate Pb less in the chemically simpler $Pb(NO_3)_2$ solutions.

However, the intercept was more strongly negative (–16.98) than in the EPA Method 1340 model, indicating a larger baseline offset between the two instruments for $Pb(NO_3)_2$ solutions. One possible explanation is that dilution of the samples for ICP analysis introduced an additional source of systematic error. The RMSE value of the training set was higher, (11.96 mg L^{-1}), which might indicate relatively poor prediction accuracy. The MAE was also high, at 4.0360 mg L^{-1}. However, model overfitting was not an issue as the validation set RMSE (6.557 mg L^{-1}) was lower than that of the training set. The high RMSE value might indicate that this technique could be limited to experiments where precision of ± 11.96 mg L^{-1} is acceptable.

Mehlich 3 regression results and discussion

Checks of simple linear regression assumptions

For the Mehlich 3 dataset, the assumptions of simple linear regression were not met. Although scatterplots suggested an approximately linear relationship between ICP and XRF values, the residuals versus fitted values plot revealed a pronounced fanning pattern, indicating heteroscedasticity.

Formal statistical tests confirmed these violations. The Anderson–Darling test rejected the null hypothesis of normality ($p < 0.005$), and both Bonett's and Levene's tests for equal variances gave $p = 0.002$, providing strong evidence of unequal variances. Similarly, the Breusch–Pagan test confirmed heteroscedasticity ($p = 4.09 \times 10^{-6}$).

The Breusch–Pagan statistic was calculated as follows: with residuals squared, the error sum of squares (SSE) was 63.94 and the regression sum of squares (SSR*) was 184.951. The chi-square value was calculated to be:

$$\chi^{2*} = \frac{\frac{SSR^*}{2}}{\left(\frac{SSE}{n}\right)^2} = \frac{\frac{184.951}{2}}{\left(\frac{63.94}{45}\right)^2} = 21.22025$$

To address these violations, two high-leverage points with unusually large residuals and the two lowest predictor values were removed, and both the predictor and response variables were log-transformed. The resulting log–log model met regression assumptions and was used in subsequent analyses.

In summary, both the EPA Method 1340 and $Pb(NO_3)_2$ datasets satisfied the assumptions of simple linear regression, supporting the validity of their models without data transformation. In contrast, the Mehlich 3 dataset violated assumptions of normality and equal variance, necessitating the removal of outliers and the application of a log–log transformation. This adjustment produced a model that better met

regression requirements and was used in subsequent analyses. The residuals vs. fits plot showed a much more random pattern, and the p-value for the Anderson-Darling test was 0.722.

Regression results

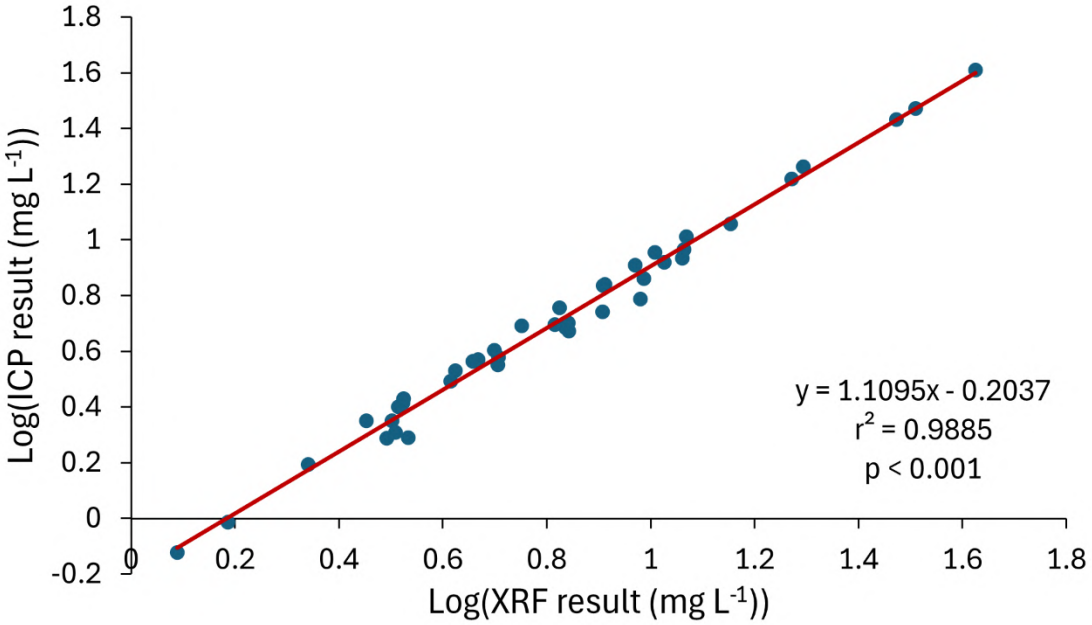

Figure 4-5. Linear regression scatterplot of log-transformed benchtop EDXRF results (average of 3 measurements) and log-transformed ICP results for Pb in Mehlich 3 soil extracts. N = 41.

For Mehlich 3 solutions, the regression equation was:

$$log(ICP\ (mg\ L^{-1})) = -0.2037 + 1.1095 \times log(XRF\ (mg\ L^{-1})).$$

The slope was 1.095 with a 95% confidence interval of (1.071, 1.148) and a p-value of < 0.001. The y-intercept was -0.2037 with a 95% confidence interval of (-0.2379, -0.1695) and a p-value of < 0.001. The model's r^2 value was 98.85% with an overall p-value of < 0.001. The RMSE was 0.0409. Back-transforming several of these statistics is required to both use the model and compare the model to the other two solutions. Upon back-transformation, we have a slope of 12.87, an intercept of 0.6256, and a RMSE of 1.0990 mg L^{-1}.

Model validation results

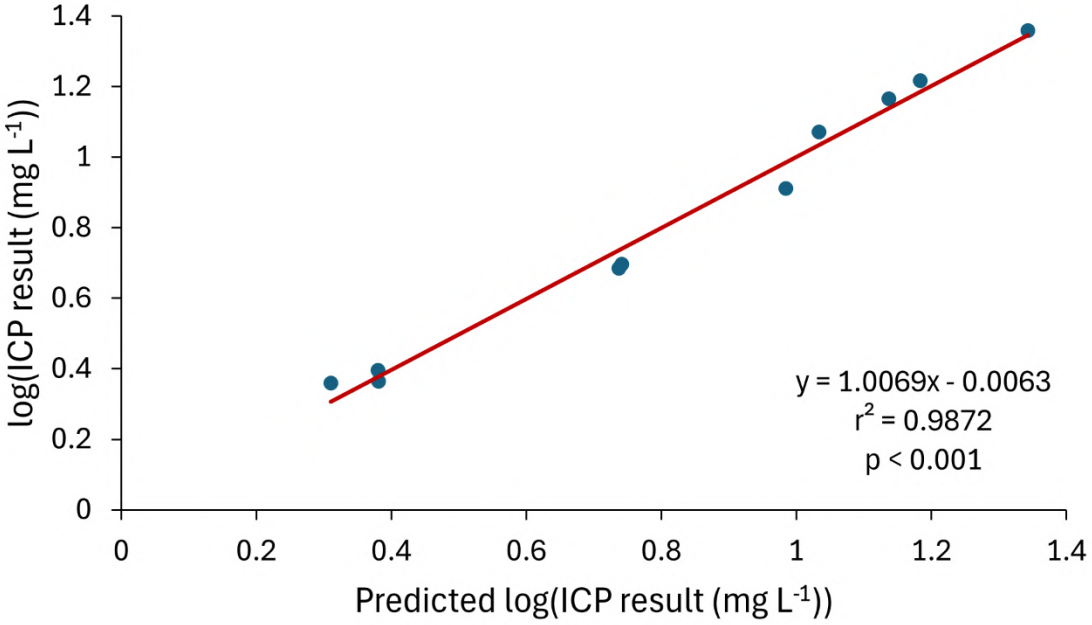

Figure 4-6. Linear regression scatterplot of the validation dataset for Pb measured in Mehlich 3 extracts. The predicted ICP result was obtained using log-transformed EDXRF measurements entered into the regression model built using the training dataset (Figure 4-5). N = 10.

The validation regression equation was:

$$\log(ICP_M) = -0.0063 + 1.0069 \times \log(ICP_C)$$

where ICP_M is the measured ICP result and ICP_C is the expected ICP result calculated by entering the XRF result into the training regression equation.

The slope was 1.0069 with a 95% confidence interval of 0.9133 to 1.1005 (back-transformed to a slope of 10.160) and a p-value of < 0.001. The y-intercept was -0.0063 with a 95% confidence interval of -0.0900 to 0.0774 (back-transformed to a slope of 0.9856) and a p-value of 0.866. This high p-value means that we cannot reject the null hypothesis that the y-intercept is equal to 0 (meaning an intercept of 1 after back-transformation). The model's r^2 value was 98.72% with an overall p-value of < 0.001. The RMSE was 0.0452 (back-transformed to 1.1097) and the MAE was 0.03598 (back-transformed to 1.0864).

Discussion

For Mehlich 3 extracts, after log–log transformation, the slope was 1.1095 (95% CI: 1.071 to 1.148) with an intercept of –0.2037 (95% CI: –0.2379 to –0.1695), with XRF results accounting for 98.85% of the variance in ICP results and an RMSE of 0.04099 (Figure 4-5).

The validation model showed a strong relationship ($r^2 = 0.98$, $p < 0.001$), indicating good predictive ability of the training model (Figure 4-6). The slope of the training model was greater than unity (1.1095, back-transformed to 12.87, Figure 4-5), indicating that XRF may underestimate Pb concentrations in Mehlich 3 extracts to a greater extent than in EPA Method 1340 or $Pb(NO_3)_2$ solutions. The intercept (–0.2037), equivalent to approximately 0.6256 mg L^{-1} after back-transformation, suggests a modest baseline offset—smaller than that observed for $Pb(NO_3)_2$ but larger than for EPA Method 1340. This model also contained several influential points that were removed, which likely contributed to the initial violations of regression assumptions and the subsequent need for log transformation. The RMSE (0.04099, back-transformed to 1.0990 mg L^{-1}) was intermediate between the other two models and lower than that of the validation set (0.0452, back-transformed to 1.1097 mg L^{-1}), indicating that overfitting was not an issue. The validation MAE (0.03598, back-transformed to 1.0864) was also intermediate. The RMSE value might indicate that this technique could be limited to experiments where precision of ± 1.0990 mg L^{-1} is acceptable.

Summary of regression models

Table 4-2 summarizes simple linear regression analysis between ICP and XRF for the 3 solutions used in this study. Regression models demonstrated strong agreement between XRF and ICP measurements across all three solution matrices. All models had high coefficients of determination ($r^2 >$ 0.98), confirming that XRF values are highly predictive of ICP results. Nevertheless, the negative

intercepts (with the exception of the Mehlich 3 model intercept) and slopes greater than unity indicate systematic biases, with XRF tending to underestimate Pb relative to ICP at higher concentrations. RMSE was lowest for EPA Method 1340 (0.2811 mg L^{-1}) and highest for $Pb(NO_3)_2$ (11.96 mg L^{-1}). The validation MAE values followed this trend, with the EPA Method 1340 model having better predictive ability than the $Pb(NO_3)_2$ model. Mehlich 3 solutions were intermediate in both RMSE and validation MAE values.

Table 4-2. Regression statistics summary predicting ICP by XRF for the three solution matrices.

Solution	N	Slope*	Y Intercept*	r^2	Model p-value	RMSE**	Validation MAE***
EPA Method 1340	30	1.4412 (1.369, 1.513)	-0.548 (-0.770, -0.320)	0.9835	< 0.001	0.2811	0.0918
Pb (II) nitrate	30	1.147 (1.128, 1.166)	-16.98 (-25.70, -8.26)	0.9982	< 0.001	11.96	4.0360
Mehlich 3****	41	12.87 (11.78, 14.06)	0.6256 (0.5782, 0.6769)	0.9885	< 0.001	1.099	1.0864

*Data is presented within a 95% confidence interval
** RMSE = root mean square error
*** MAE = mean absolute error
**** Slope, intercept, and RMSE are back-transformed

Future work

Further investigation is needed to determine the utility of benchtop EDXRF on liquid environmental samples. It is important to note that soil samples with varying chemical compositions may result in bioaccessibility extractions containing different solutes, which in high enough concentrations could affect XRF accuracy. Therefore, expanding the sample pool to include additional soils, or separating soils by properties, could yield more accurate regression models for such digestions. Larger sample sizes could improve the accuracy of the three regression models presented here for EPA Method 1340, $Pb(NO_3)_2$, and Mehlich 3 matrices. Alternative XRF methods such as different instrument settings, calibrations, or sample preparation could be developed. XRF analysis of other matrices (e.g., EPA Method 3050B total soil Pb digestions) and different heavy metals should also be explored.

Conclusions

This study evaluated the performance of benchtop energy-dispersive X-ray fluorescence spectroscopy (XRF) for quantifying Pb in three common aqueous extractants—EPA Method 1340 soil extracts, $Pb(NO_3)_2$ solutions, and Mehlich 3 soil extracts—by comparison with ICP.

Across all matrices, XRF exhibited strong agreement with ICP results ($r^2 > 0.98$), with validation confirming predictive reliability. Detection limits (0.17 - 0.25 mg L^{-1}), quantification limits (0.509 - 0.751 mg L^{-1}), and reproducibility (standard deviations as low as 0.055 mg L^{-1}) indicate that XRF is suitable for aqueous Pb determinations within the concentration ranges typically encountered in environmental assessments.

Systematic biases were observed, including slopes greater than unity and negative intercepts, which suggest that raw XRF values tend to underestimate Pb concentrations relative to ICP, particularly at higher concentrations. These biases underscore the importance of regression calibration before applying XRF data in practice. Further, the magnitude of error (RMSE 0.2811 - 11.96 mg L^{-1}) indicates the level of precision that must be acceptable to use XRF for Pb measurement.

Overall, calibrated XRF shows potential to provide a rapid, cost-effective, and accessible alternative for quantifying Pb in environmental solutions, with particular utility for community laboratories, field-based research, and resource-limited settings. By enabling rapid and affordable Pb measurements in soil extracts, XRF could expand environmental testing capacity for urban gardening, public health monitoring, and community-led remediation projects where access to conventional laboratory infrastructure is limited.

Chapter 5

Summary

This study presents an evaluation of biochar modification for lead (Pb) immobilization and the application of benchtop energy-dispersive X-ray fluorescence spectroscopy (XRF) for Pb analysis in liquid samples. Our findings demonstrate the potential for biochar-based materials and XRF methods to enhance environmental remediation and monitoring efforts, while also highlighting the need for further refinement to optimize their practical application.

The oxidative modification of wood chip-based biochar in air at 300°C led to significant physical and chemical changes, including an increase in specific surface area, pore development, and the introduction of oxygenated functional groups. In addition, enhanced Pb(II) sorption capacity was seen in biochar sorption experiments. The results suggest that the modification process creates additional acidic sites, such as –COOH and –C=O, which facilitate stronger interactions with Pb(II) at the biochar surface.

However, when applied in biochar-amended soils under more realistic conditions, the impact of biochar on Pb immobilization was less pronounced. Three experiments revealed that biochar treatments did not consistently reduce bioaccessible Pb in soil. In fact, at one sampling point, biochar amendments were found to increase bioaccessible Pb, contrary to our initial hypothesis. The study included a variety of biochar treatments, ranging from unheated to thermally modified biochar (at 300°C for 1–4 hours), and tested different Pb contamination levels. The results indicated that biochar's performance as a Pb immobilization agent was highly variable and influenced by soil conditions, with no significant differences observed in the majority of treatments. These findings underscore the complexity of biochar's behavior in the soil environment and suggest that biochar's effectiveness for Pb immobilization may be limited by specific environmental factors.

In parallel, the performance of benchtop XRF as an alternative method for quantifying Pb in aqueous extractants was evaluated. XRF was shown to provide reliable Pb measurements, with a high correlation to inductively coupled plasma (ICP) results ($r^2 > 0.98$). The detection limits and quantification limits (ranging from 0.17–0.25 mg L^{-1} and 0.509–0.751 mg L^{-1}, respectively) were found to be well-suited for environmental Pb concentrations typically encountered in soil extracts. Additionally, the precision of XRF was excellent, with low standard deviations (as low as 0.055 mg L^{-1}), indicating that XRF could offer a rapid, cost-effective alternative to traditional laboratory techniques. However, systematic biases, including underestimation of Pb concentrations at higher levels, were observed, which suggests the need for careful calibration when using XRF for Pb quantification. Despite these biases, the technique's reliability and accessibility make it an attractive option for field-based research, community laboratories, and low-resource settings where conventional laboratory infrastructure is limited. The ability of XRF to deliver fast and affordable Pb measurements could significantly enhance environmental testing capacities, particularly for urban gardening, public health monitoring, and community-led remediation projects.

In conclusion, the results of this study highlight the potential of heat-modified biochar as a tool for Pb immobilization in environmental remediation efforts but also emphasize the need for further investigation into its performance in complex field conditions. The variability observed in biochar's effectiveness suggests that its utility as a remediation agent will depend heavily on site-specific factors. Furthermore, the use of XRF as a practical method for Pb quantification holds promise, particularly in resource-limited environments, although calibration is critical to ensure the accuracy of results.

Appendix

Biochar Characterization

Table A-1. Characteristics of biochar used in the experiment as reported by Metzler Biochar (analyses done following IBI guidelines by Control Laboratories, Watsonville, CA).

Property	Result	Units	Method
Moisture (time of analysis)	67.1	% wet wt.	ASTM D1762-84 (105c)
Bulk Density	10.7	lb/cu ft	
Organic Carbon	78.2	% of total dry mass	Dry Combust-ASTM D 4373
Hydrogen/Carbon (H:C)	0.24 - 0.7	Molar Ratio	H dry combustion/C(above)
Total Ash	9.7	% of total dry mass	ASTM D-1762-84
Total Nitrogen	0.77	% of total dry mass	Dry Combustion
pH value	9.55	units	4.11USCC:dil. Rajkovich
Electrical Conductivity (EC20 w/w)	1.07	dS/m	4.10USCC:dil. Rajkovich
Liming (neut. Value as-CaCO3)	9.2	%CaCO3	AOAC 955.01
Carbonates (as-CaCO3)	7.2	%CaCO3	ASTM D 4373
Butane Act.	5.5	g/100g dry	ASTM D 5742-95
Surface Area Correlation	308	m^2/g dry	G
Total (K)	6267	mg/kg	E
Total (P)	882	mg/kg	E
Ammonia (NH4-N)	3.4	mg/kg	A
Nitrate (NO3-N)	0.9	mg/kg	A
Organic (Org-N)	7677	mg/kg	Calc.
Volatile Matter	21.3	percent dw	D

A: Rayment & Higginson

G: Butane Activity Surface Area Correlation Based on McLaughlin, Shields, Jagiello, & Thiele's 2012 paper: Analytical Options for Biochar Adsorption and Surface Area

D: ASTM D1762-84

E EPA3050B/EPA 6010

Table A-2. Metal content of biochar used in the experiment as reported by Metzler Biochar (analyses done following IBI guidelines by Control Laboratories, Watsonville, CA).

Metal	Result (mg L^{-1})	Range of Max. Levels (mg L^{-1})	Reporting Limit (mg L^{-1})	Method
Arsenic (As)	ND	13 to 100	0.49	EPA3050B/EPA 6020
Cadmium (Cd)	1.0	1.4 to 39	0.20	EPA3050B/EPA 6020
Chromium (Cr)	3.0	93 to 1200	0.49	EPA3050B/EPA 6020
Cobalt (Co)	1.0	34 to 100	0.49	EPA3050B/EPA 6020
Copper (Cu)	15.0	143 to 6000	0.49	EPA3050B/EPA 6020
Lead (Pb)	7.3	121 to 300	0.20	EPA3050B/EPA 6020
Molybdenum (Mo)	ND	5 to 75	0.49	EPA3050B/EPA 6020
Mercury (Hg)	ND	1 to 17	0.001	EPA 7471
Nickel (Ni)	6.4	47 to 420	0.49	EPA3050B/EPA 6020
Zinc (Zn)	33.9	416 to 7400	0.98	EPA3050B/EPA 6020
Sodium (Na)	488	Declaration	488.1	EPA3050B/EPA 6010
Iron (Fe)	1284	Declaration	24.4	EPA3050B/EPA 6010
Manganese (Mn)	1593	Declaration	0.49	EPA3050B/EPA 6020

Table A-3. Particle size distribution of the biochar used in this project as reported by Metzler Biochar (analyses done using ASTM D 2862 Granular method following IBI guidelines by Control Laboratories, Watsonville, CA).

Particle Size Distribution	Result (%)
< 0.5 mm	56.4
0.5-1 mm	26.5
1-2 mm	14.0
2-4 mm	3.1
> 4 mm	0.0

References

Amalina, F., Razak, A. S. A., Krishnan, S., Sulaiman, H., Zularisam, A. W., & Nasrullah, M. (2022). Biochar production techniques utilizing biomass waste-derived materials and environmental applications – A review. *Journal of Hazardous Materials Advances, 7*, 100134. https://doi.org/10.1016/j.hazadv.2022.100134

Antić-Mladenović, S., Frohne, T., Kresović, M., Stärk, H.-J., Tomić, Z., Ličina, V., & Rinklebe, J. (2017). Biogeochemistry of Ni and Pb in a periodically flooded arable soil: Fractionation and redox-induced (im)mobilization. *Journal of Environmental Management, 186*, 141–150. https://doi.org/10.1016/j.jenvman.2016.06.005

Bashir, S., Hussain, Q., Zhu, J., Fu, Q., Houben, D., & Hu, H. (2020a). Efficiency of KOH-modified rice straw-derived biochar for reducing cadmium mobility, bioaccessibility and bioavailability risk index in red soil. *Pedosphere*, *30*(6), 874–882. https://doi.org/10.1016/S1002-0160(20)60043-1

Bashir, S., Hussain, Q., Zhu, J., Fu, Q., Houben, D., & Hu, H. (2020b). Efficiency of KOH-modified rice straw-derived biochar for reducing cadmium mobility, bioaccessibility and bioavailability risk index in red soil. *Pedosphere*, *30*(6), 874–882. https://doi.org/10.1016/S1002-0160(20)60043-1

Behnam, H., Firouzi, A. F., & Šimůnek, J. (2024). Pb^{2+} adsorption on functionalized biochar nanoparticles: Insights from nanoparticle characterization and kinetic-isotherm analysis. *Soil Science Society of America Journal*, *88*(3), 700–717. https://doi.org/10.1002/saj2.20669

Birch, H. F. (1958). The effect of soil drying on humus decomposition and nitrogen availability. *Plant and Soil*, *10*(1), 9–31. https://doi.org/10.1007/BF01343734

Bolan, N., Kunhikrishnan, A., Thangarajan, R., Kumpiene, J., Park, J., Makino, T., Kirkham, M. B., & Scheckel, K. (2014). Remediation of heavy metal(loid)s contaminated soils – To mobilize or to immobilize? *Journal of Hazardous Materials*, *266*, 141–166. https://doi.org/10.1016/j.jhazmat.2013.12.018

Byers, H. L., McHenry, L. J., & Grundl, T. J. (2020). Increased risk for lead exposure in children through consumption of produce grown in urban soils. *The Science of the Total Environment*, *743*, 140414. https://doi.org/10.1016/j.scitotenv.2020.140414

Childhood Lead Poisoning Prevention: Populations at Higher Risk. (2021). Centers for Disease Control and Prevention. https://www.cdc.gov/nceh/lead/prevention/populations.htm

Chojnacka, K., Samoraj, M., Tuhy, Ł., Michalak, I., Mironiuk, M., & Mikulewicz, M. (2018). Using XRF and ICP-OES in Biosorption Studies. Molecules (Basel, Switzerland), 23(8), 2076. https://doi.org/10.3390/molecules23082076

Dadio, S. (2024). *An Investigation of Elemental Soil Composition Testing Methods and Site Assessment Procedure for Determining Trace Elemental Pollutant Concentrations in Urban Soils* [The Pennsylvania State University]. https://etda.libraries.psu.edu/catalog/27842sqd5560

Dong, Y., Ma, L. Q., & Rhue, R. D. (2000). Relation of enhanced Pb solubility to Fe partitioning in soils. *Environmental Pollution*, *110*(3), 515–522. https://doi.org/10.1016/S0269-7491(99)00312-7

Drexler, J. W., & Brattin, W. J. (2007). An *In Vitro* Procedure for Estimation of Lead Relative Bioavailability: With Validation. *Human and Ecological Risk Assessment: An International Journal*, *13*(2), 383–401. https://doi.org/10.1080/10807030701226350

Elbana, T. A., Magdi Selim, H., Akrami, N., Newman, A., Shaheen, S. M., & Rinklebe, J. (2018). Freundlich sorption parameters for cadmium, copper, nickel, lead, and zinc for different soils: Influence of kinetics. *Geoderma*, *324*, 80–88. https://doi.org/10.1016/j.geoderma.2018.03.019

Energy Dispersive X-ray Fluorescence Spectrometer. (2023). *Rigaku Journal*, *39*(1), 35–37.

Furman, O., Strawn, D. G., & McGeehan, S. (2007). Sample Drying Effects on Lead Bioaccessibility in Reduced Soil. *Journal of Environmental Quality*, *36*(3), 899–903. https://doi.org/10.2134/jeq2006.0340

Gee, G. W., & Bauder, J. W. (1986). Particle-Size Analysis. In *Methods of Soil Analysis* (2nd ed., pp. 383–411). Soil Science Society of America. https://www.scirp.org/reference/ReferencesPapers?ReferenceID=1898399

Gee, G. W., & Or, D. (2018). Particle-Size Analysis. In J. H. Dane & G. Clarke Topp (Eds.), *SSSA Book Series* (pp. 255–293). Soil Science Society of America. https://doi.org/10.2136/sssabookser5.4.c12

Hamel, S. C., Heckman, J. R., Shilke-Gartley, K. L., & Hoskins, B. (2003). Lead Extraction Using Three Soil Fertility Tests and Environmental Protection Agency Method 3050. *Communications in Soil Science and Plant Analysis*, *34*(19–20), 2853–2873. https://doi.org/10.1081/CSS-120025211

Hanna, A. K., & Oh, P. (2000). Rethinking Urban Poverty: A Look at Community Gardens. *Bulletin of Science, Technology & Society*, *20*(3), 207–216. https://doi.org/10.1177/027046760002000308

He, L., Zhong, H., Liu, G., Dai, Z., Brookes, P. C., & Xu, J. (2019). Remediation of heavy metal contaminated soils by biochar: Mechanisms, potential risks and applications in China. *Environmental Pollution*, *252*, 846–855. https://doi.org/10.1016/j.envpol.2019.05.151

Horst, M., McClintock, N., & Hoey, L. (2017). The Intersection of Planning, Urban Agriculture, and Food Justice: A Review of the Literature. *Journal of the American Planning Association*, *83*(3), 277–295. https://doi.org/10.1080/01944363.2017.1322914

Huang, H., Guan, H., Tian, Z.-Q., Chen, M.-M., Tian, K.-K., Zhao, F.-J., & Wang, P. (2024). Exposure sources, intake pathways and accumulation of lead in human blood. *Soil Security*, *15*, 100150. https://doi.org/10.1016/j.soisec.2024.100150

Huang, X., Chang, M., Han, L., Li, J., Li, S.-W., & Li, H.-B. (2023). Variation of lead bioaccessibility in soil reference materials: Intra- and inter-laboratory assessments. *Chemosphere*, *312*, 137293. https://doi.org/10.1016/j.chemosphere.2022.137293

Husson, O. (2013). Redox potential (Eh) and pH as drivers of soil/plant/microorganism systems: A transdisciplinary overview pointing to integrative opportunities for agronomy. *Plant and Soil*, *362*(1–2), 389–417. https://doi.org/10.1007/s11104-012-1429-7

Kassambara, A. (2025). *Ggplot2 package* (Version 0.6.2) [Computer software]. https://rpkgs.datanovia.com/ggpubr/

Kim, B. F., Poulsen, M. N., Margulies, J. D., Dix, K. L., Palmer, A. M., & Nachman, K. E. (2014). Urban Community Gardeners' Knowledge and Perceptions of Soil Contaminant Risks. *PLoS ONE*, *9*(2), e87913. https://doi.org/10.1371/journal.pone.0087913

Klüpfel, L., Keiluweit, M., Kleber, M., & Sander, M. (2014). Redox Properties of Plant Biomass-Derived Black Carbon (Biochar). *Environmental Science & Technology*, *48*(10), 5601–5611. https://doi.org/10.1021/es500906d

Kumar, S., Rahman, Md. A., Islam, Md. R., Hashem, Md. A., & Rahman, M. M. (2022). Lead and other elements-based pollution in soil, crops and water near a lead-acid battery recycling factory in Bangladesh. *Chemosphere*, *290*, 133288. https://doi.org/10.1016/j.chemosphere.2021.133288

Laidlaw, M. A. S., & Filippelli, G. M. (2008). Resuspension of urban soils as a persistent source of lead poisoning in children: A review and new directions. *Applied Geochemistry*, *23*(8), 2021–2039. https://doi.org/10.1016/j.apgeochem.2008.05.009

Laidlaw, M. A. S., Filippelli, G. M., Sadler, R. C., Gonzales, C. R., Ball, A. S., & Mielke, H. W. (2016). Children's Blood Lead Seasonality in Flint, Michigan (USA), and Soil-Sourced Lead Hazard Risks. *International Journal of Environmental Research and Public Health*, *13*(4), 358. https://doi.org/10.3390/ijerph13040358

Landes, F. C., Calcio, M., Sobolewski, J. M., Wallens-Logan, K., Ledeczi, A., Kiro, Y., Bolge, L., Ross, J., Chillrud, S. N., Mailloux, B. J., & Geen, A. van. (2023). Widespread Pb contamination in urban backyard soils for >100 years identified in soil cores constrained by 210Pb and 137Cs. *Science of The Total Environment*, *899*, 165407. https://doi.org/10.1016/j.scitotenv.2023.165407

Lead in Soil. (2020). US Environmental Protection Agency. https://www.epa.gov/sites/default/files/2020-10/documents/lead-in-soil-aug2020.pdf

Leon y Leon, C., & Radovic, L. R. (1993). Interfacial Chemistry and Electrochemistry of Carbon Surfaces. In *Chemistry & Physics of Carbon* (1st ed., Vol. 24, pp. 213–292). CRC Press.

Levin, R. (2016). The attributable annual health costs of U.S. occupational lead poisoning. *International Journal of Occupational and Environmental Health*, *22*(2), 107–120. https://doi.org/10.1080/10773525.2016.1173945

Li, Y., Liu, J., Wang, Y., Tang, X., Xu, J., & Liu, X. (2023). Contribution of components in natural soil to Cd and Pb competitive adsorption: Semi-quantitative to quantitative analysis. *Journal of Hazardous Materials*, *441*, 129883. https://doi.org/10.1016/j.jhazmat.2022.129883

Li, Y., Wu, J., Qian, J., Sun, J., Huang, T., Li, H., & Chen, X. (2023). Environmental remediation of Pb–Cd contaminated soil with organic phosphonic acids-saponin: Conditions, effectiveness, ecological risk and recovery. *Chemosphere*, *322*, 138122. https://doi.org/10.1016/j.chemosphere.2023.138122

Lusby, G., Hall, C., & Reiners, J. (2015). Lead Contamination of Surface Soils in Philadelphia from Lead Smelters and Urbanization. *Environmental Justice*, *8*(1), 6–14. https://doi.org/10.1089/env.2014.0008

Al Maliki, A., Al-lami, A.K., Hussain, H.M., Al-Ansari, N. (2017). Comparison between inductively coupled plasma and X-ray fluorescence performance for Pb analysis in environmental soil samples. *Environ Earth Sci, 76*(433). https://doi.org/10.1007/s12665-017-6753-z

Marguí, E., Queralt, I., & de Almeida, E. (2022). X-ray fluorescence spectrometry for environmental analysis: Basic principles, instrumentation, applications and recent trends. *Chemosphere*, *303*, 135006. https://doi.org/10.1016/j.chemosphere.2022.135006

Marguí, E., Zawisza, B., & Sitko, R. (2014). Trace and ultratrace analysis of liquid samples by X-ray fluorescence spectrometry. *TrAC Trends in Analytical Chemistry, 53*, 73–83. https://doi.org/10.1016/j.trac.2013.09.009

Marriott, B. (2025). *How Much Does an XRF Spectrometer Cost?* Rigaku. https://rigaku.com/products/xrf-spectrometers/learning/blog/how-much-does-an-xrf-spectrometer-cost

Masson, G., Ugwu, E., Martínez-Villegas, N., & Sen Gupta, B. (2025). Remediation of Lead-Contaminated Soil by Using Saponin Derived from Sapindus Mukorossi. *European Journal of Environment and Earth Sciences*, *3*. https://doi.org/10.24018/ejgeo.2022.3.3.293

McBride, M., Sauve, S., & Hendershot, W. (1997). Solubility control of Cu, Zn, Cd and Pb in contaminated soils. *European Journal of Soil Science, 48*(2), 337–346. https://doi.org/10.1111/j.1365-2389.1997.tb00554.x

Mehlich, A. (1984). Mehlich 3 soil test extractant: A modification of Mehlich 2 extractant. *Communications in Soil Science and Plant Analysis*, *15*(12), 1409–1416. https://doi.org/10.1080/00103628409367568

Mielke, H. W., Gonzales, C. R., Powell, E. T., & Egendorf, S. P. (2022). Lead in Air, Soil, and Blood: Pb Poisoning in a Changing World. *International Journal of Environmental Research and Public Health*, *19*(15), 9500. https://doi.org/10.3390/ijerph19159500

Minca, K. K., Basta, N. T., & Scheckel, K. G. (2013). Using the Mehlich-3 Soil Test as an Inexpensive Screening Tool to Estimate Total and Bioaccessible Lead in Urban Soils. *Journal of Environmental Quality*, *42*(5), 1518–1526. https://doi.org/10.2134/jeq2012.0450

Minitab, LLC. (2023). *Minitab Statistical Software* (Version 21) [Computer software]. www.minitab.com

Moradi, M., Yamini, Y., Kakehmam, J., & Ahmadi, K. (2015). A review in the sample preparation of aqueous solutions combined with X-ray fluorescence detection. *Journal of the Iranian Chemical Society*, *12*(5), 831–838. https://doi.org/10.1007/s13738-014-0545-0

O'Shea, M. J., Krekeler, M. P. S., Vann, D. R., & Gieré, R. (2021). Investigation of Pb-contaminated soil and road dust in a polluted area of Philadelphia. *Environmental Monitoring and Assessment*, *193*(7), 440. https://doi.org/10.1007/s10661-021-09213-9

Pais, I., & Jones, B. (1998). The Handbook of Trace Elements. *Journal of Environmental Quality*, *27*(4), 986–986. https://doi.org/10.2134/jeq1998.00472425002700040041x

Paltseva, A., & Cheng, Z. (2018). Rapid Screening of Bioaccessible Pb in Urban Soils Using pXRF. *Springer Geography*.

Pignatello, J. J., Uchimiya, M., & Abiven, S. (2024). Aging of biochar in soils and its implications. In *Biochar for Environmental Management* (3rd ed.). Routledge.

Plunkett, S. A., Eckley, C. S., Luxton, T. P., & Johnson, M. G. (2022). The effects of biochar and redox conditions on soil Pb bioaccessibility to people and waterfowl. *Chemosphere*, *294*, 133675. https://doi.org/10.1016/j.chemosphere.2022.133675

Pourrut, B., Shahid, M., Dumat, C., Winterton, P., & Pinelli, E. (2011). Lead Uptake, Toxicity, and Detoxification in Plants. In D. M. Whitacre (Ed.), *Reviews of Environmental Contamination and Toxicology Volume 213* (Vol. 213, pp. 113–136). Springer New York. https://doi.org/10.1007/978-1-4419-9860-6_4

Priya, A. K., Muruganandam, M., Ali, S. S., & Kornaros, M. (2023). Clean-Up of Heavy Metals from Contaminated Soil by Phytoremediation: A Multidisciplinary and Eco-Friendly Approach. *Toxics*, *11*(5), 422. https://doi.org/10.3390/toxics11050422

Pyle, S. M., Nocerino, J. M., Deming, S. N., Palasota, J. A., Palasota, J. M., Miller, E. L., Hillman, D. C., Kuharic, C. A., Cole, W. H., Fitzpatrick, P. M., Watson, M. A., & Nichols, K. D. (1996). Comparison of AAS, ICP-AES, PSA, and XRF in Determining Lead and Cadmium in Soil. *Environmental Science & Technology*, *30*(1), 204–213. https://doi.org/10.1021/es9502482

Rajkovich, S., Enders, A., Hanley, K., Hyland, C., Zimmerman, A. R., & Lehmann, J. (2012). Corn growth and nitrogen nutrition after additions of biochars with varying properties to a temperate soil. *Biology and Fertility of Soils*, *48*(3), 271–284. https://doi.org/10.1007/s00374-011-0624-7

Ramsey, M.H., Potts, P.J., Webb, P.C., Watkins, P., Watson, J.S., Coles, B.J. (1995). An objective assessment of analytical method precision: comparison of ICP-AES and XRF for the analysis of silicate rocks. *Chemical Geology,124*(1-2), 1-19. https://doi.org/10.1016/0009-2541(95)00020-M

Rees, F., Simonnot, M. O., & Morel, J. L. (2014). Short-term effects of biochar on soil heavy metal mobility are controlled by intra-particle diffusion and soil pH increase. *European Journal of Soil Science*, *65*(1), 149–161. https://doi.org/10.1111/ejss.12107

Sauvé, S., McBride, M., & Hendershot, W. (1998). Soil Solution Speciation of Lead(II): Effects of Organic Matter and pH. *Soil Science Society of America Journal*, *62*(3), 618–621. https://doi.org/10.2136/sssaj1998.03615995006200030010x

Schulte, E. E., & Hoskins, B. (2011). Recommended Soil Organic Matter Tests. In J. T. Sims & A. Wolf (Eds.), *Recommended Soil Testing Procedures for the Northeastern United States* (3rd ed., pp. 63–74).

Schupp, T., Damm, G., Foth, H., Freyberger, A., Gebel, T., Gundert-Remy, U., Hengstler, J. G., Mangerich, A., Partosch, F., Röhl, C., & Wollin, K.-M. (2020). Long-term simulation of lead concentrations in agricultural soils in relation to human adverse health effects. *Archives of Toxicology*, *94*(7), 2319–2329. https://doi.org/10.1007/s00204-020-02762-x

Sivaranjanee, R., Kumar, P. S., & Rangasamy, G. (2023). A critical review on biochar for environmental applications. *Carbon Letters*, *33*(5), 1407–1432. https://doi.org/10.1007/s42823-023-00527-x

Skopp, J., Jawson, M. D., & Doran, J. W. (1990). Steady-State Aerobic Microbial Activity as a Function of Soil Water Content. *Soil Science Society of America Journal*, *54*(6), 1619–1625. https://doi.org/10.2136/sssaj1990.03615995005400060018x

Small, G., Shrestha, P., Metson, G. S., Polsky, K., Jimenez, I., & Kay, A. (2019). Excess phosphorus from compost applications in urban gardens creates potential pollution hotspots. *Environmental Research Communications*, *1*(9), 091007. https://doi.org/10.1088/2515-7620/ab3b8c

Soil contaminants: Lead. (2024). Soil Science Society of America. https://www.soils.org/about-soils/contaminants/lead/

Sources of Lead Exposure. (2023). Centers for Disease Control and Prevention. https://www.cdc.gov/nceh/lead/prevention/sources.htm

Stumm, W., & Morgan, J. J. (1996). *Aquatic chemistry: Chemical equilibria and rates in natural waters* (Third edition). John Wiley & Sons, Inc.

Sun, T., Levin, B. D. A., Guzman, J. J. L., Enders, A., Muller, D. A., Angenent, L. T., & Lehmann, J. (2017). Rapid electron transfer by the carbon matrix in natural pyrogenic carbon. *Nature Communications*, *8*(1), 14873. https://doi.org/10.1038/ncomms14873

Sun, Z., Dai, L., Lai, P., Shen, F., Shen, F., & Zhu, W. (2022). Air oxidation in surface engineering of biochar-based materials: A critical review. *Carbon Research*, *1*(1), 32. https://doi.org/10.1007/s44246-022-00031-3

Tan, G., & Yu, H.-Q. (2023). Rethinking biochar: Black gold or not? *Nature Reviews Materials*, *9*(1), 4–5. https://doi.org/10.1038/s41578-023-00634-1

Thomas, R. (2016). *Money To Burn: Do you Know What is Costs to Run your Atomic Spectroscopy instrumentation?* www.researchgate.net/publication/330262373_Money_To_Burn_Do_you_Know_What_is_Costs_to_Run_your_Atomic_Spectroscopy_instrumentation

Thommes, M., Kaneko, K., Neimark, A. V., Olivier, J. P., Rodriguez-Reinoso, F., Rouquerol, J., & Sing, K. S. W. (2015). Physisorption of gases, with special reference to the evaluation of surface area and pore size distribution (IUPAC Technical Report). *Pure and Applied Chemistry*, *87*(9–10), 1051–1069. https://doi.org/doi:10.1515/pac-2014-1117

Tipping, E. (2002). *Cation Binding by Humic Substances* (1st ed.). Cambridge University Press. https://doi.org/10.1017/CBO9780511535598

Urban Agriculture. (n.d.). U.S. Department of Agriculture. https://www.climatehubs.usda.gov/hubs/international/topic/urban-agriculture

US EPA. (2007). *Estimation of relative bioavailability of lead in soil and soil-like materials using in vivo and in vitro methods*. US Environmental Protection Agency. https://semspub.epa.gov/work/11/175416.pdf

US EPA. (1996a, December). *METHOD 3050B ACID DIGESTION OF SEDIMENTS, SLUDGES, AND SOILS*. US Environmental Protection Agency. http://epa.gov/hw-sw846/sw-846-test-method-3050b-acid-digestion-sediments-sludges-and-soils

US EPA. (1996b, December). *METHOD 6010B INDUCTIVELY COUPLED PLASMA-ATOMIC EMISSION SPECTROMETRY*. US Environmental Protection Agency. https://www.epa.gov/sites/default/files/documents/6010b.pdf

US EPA. (2013, February 12). *Protect Your Family from Sources of Lead* [Overviews and Factsheets]. https://www.epa.gov/lead/protect-your-family-sources-lead

US EPA. (2017). *METHOD 1340 IN VITRO BIOACCESSIBILITY ASSAY FOR LEAD IN SOIL*. US Environmental Protection Agency. https://www.epa.gov/sites/default/files/2017-03/documents/method_1340_update_vi_final_3-22-17.pdf

US EPA. (2021). *Fact Sheet: Lead RBA and IVBA*. US Environmental Protection Agency. https://semspub.epa.gov/work/HQ/100002717.pdf

US EPA. (2024a). *EPA Strengthens Safeguards to Protect Families and Children from Lead in Contaminated Soil at Residential Sites in Region 7*. US Environmental Protection Agency. https://epa.gov/newsreleases/epa-strengthens-safeguards-protect-families-and-children-lead-contaminated-soil

US EPA. (2024b). *Environmental Justice*. US Environmental Protection Agency. https://www.epa.gov/environmentaljustice

Wagner, F., & Payne, L. (2019). Growing Local: The Role of Urban Gardening in Fostering Food Security, Sustainability, and Community. *Purdue Journal of Service Learning and International Engagement*, *6*(1). https://doi.org/10.5703/1288284316991

Wharton, S. E., Shayler, H. A., Spliethoff, H. M., Marquez-Bravo, L. G., Ribaudo, L., & McBride, M. B. (2012). A Comparison of Screening Tests for Soil Pb. *Soil Science*, *177*(11), 650–654. https://doi.org/10.1097/SS.0b013e318277718b

Whitehead, L. S., & Buchanan, S. D. (2019). Childhood Lead Poisoning: A Perpetual Environmental Justice Issue? *Journal of Public Health Management and Practice*, *25*, S115. https://doi.org/10.1097/PHH.0000000000000891

Wilbur, S. (2005). *A Comparison of the Relative Cost and Productivity of Traditional Metals Analysis Techniques Versus ICP-MS in High Throughput Commercial Laboratories.* Agilent Technologies.

Wolf and Beegle. (2011). Recommended soil tests for macronutrients. In *Recommended Soil Testing Procedures for the Northeastern United States* (3rd ed., pp. 39–47). Agricultural Experiment Station, University of Delaware, Newark, DE.

Xie, R., Jin, Y., Chen, Y., & Jiang, W. (2017). The importance of surface functional groups in the adsorption of copper onto walnut shell derived activated carbon. *Water Science and Technology: A Journal of the International Association on Water Pollution Research*, *76*(11–12), 3022–3034. https://doi.org/10.2166/wst.2017.471

Yan, K., Dong, Z., Liu, Y., & Naidu, R. (2016). Quantifying statistical relationships between commonly used in vitro models for estimating lead bioaccessibility. *Environmental Science and Pollution Research*, *23*(7), 6873–6882. https://doi.org/10.1007/s11356-015-5947-8

Yang, J.K., Barnett, M. O., Jardine, P. M., & Brooks, S. C. (2003). Factors Controlling the Bioaccessibility of Arsenic(V) and Lead(II) in Soil. *Soil and Sediment Contamination: An International Journal*, *12*(2), 165–179. https://doi.org/10.1080/713610968

Yang, X., Pan, H., Shaheen, S. M., Wang, H., & Rinklebe, J. (2021). Immobilization of cadmium and lead using phosphorus-rich animal-derived and iron-modified plant-derived biochars under dynamic redox conditions in a paddy soil. *Environment International*, *156*, 106628. https://doi.org/10.1016/j.envint.2021.106628

Yuan, C., Gao, B., Peng, Y., Gao, X., Fan, B., & Chen, Q. (2021). A meta-analysis of heavy metal bioavailability response to biochar aging: Importance of soil and biochar properties. *Science of The Total Environment*, *756*, 144058. https://doi.org/10.1016/j.scitotenv.2020.144058

Yuan, P., Wang, J., Pan, Y., Shen, B., & Wu, C. (2019). Review of biochar for the management of contaminated soil: Preparation, application and prospect. *Science of The Total Environment*, *659*, 473–490. https://doi.org/10.1016/j.scitotenv.2018.12.400

Yuan, Y., Bolan, N., Prévoteau, A., Vithanage, M., Biswas, J. K., Ok, Y. S., & Wang, H. (2017). Applications of biochar in redox-mediated reactions. *Bioresource Technology*, *246*, 271–281. https://doi.org/10.1016/j.biortech.2017.06.154

Zhao, J., Shen, X.-J., Domene, X., Alcañiz, J.-M., Liao, X., & Palet, C. (2019). Comparison of biochars derived from different types of feedstock and their potential for heavy metal removal in multiple-metal solutions. *Scientific Reports*, *9*(1), 9869. https://doi.org/10.1038/s41598-019-46234-4

Zia, M. H., Codling, E. E., Scheckel, K. G., & Chaney, R. L. (2011). In vitro and in vivo approaches for the measurement of oral bioavailability of lead (Pb) in contaminated soils: A review. *Environmental Pollution*, *159*(10), 2320–2327. https://doi.org/10.1016/j.envpol.2011.04.043